# ORIGINAL RESEARCH

ATF2 and ATF7 Are Critical Mediators of Intestinal Epithelial Repair

Bartolomeus J. Meijer,[1] Francesca P. Giugliano,[1] Bart Baan,[1] Jonathan H. M. van der Meer,[1] Sander Meisner,[1] Manon van Roest,[1] Pim J. Koelink,[1] Ruben J. de Boer,[1] Nic Jones,[2] Wolfgang Breitwieser,[3] Nicole N. van der Wel,[4] Manon E. Wildenberg,[1] Gijs R. van den Brink,[1,5] Jarom Heijmans,[1,6] and Vanesa Muncan[1]

[1]Department of Gastroenterology and Hepatology, Amsterdam Gastroenterology & Metabolism, Tytgat Institute for Liver and Intestinal Research, [4]Department of Medical Biology, Electron Microscopy Center Amsterdam, [6]Department of Internal Medicine, Amsterdam University Medical Center, University of Amsterdam, Amsterdam, The Netherlands; [2]Department of Cell Regulation, [3]Department of Cell Regulation, Cancer Research United Kingdom Manchester Institute, University of Manchester, Manchester, United Kingdom; [5]Roche Innovation Center Basel, F. Hoffmann-La Roche Associate Group, Basel, Switzerland
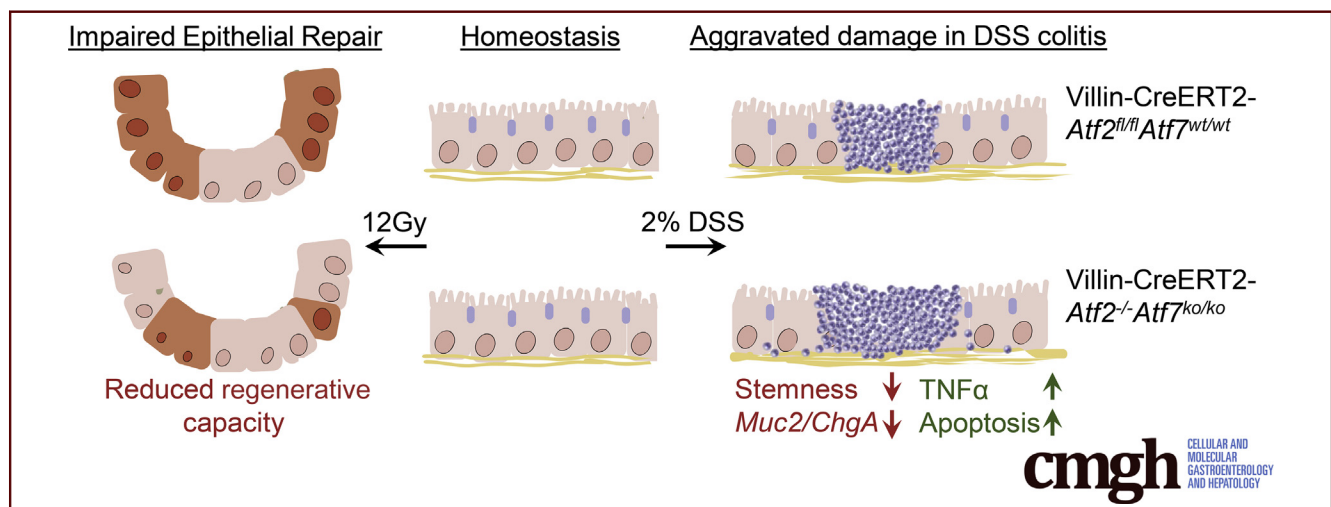
SUMMARY

We show that ATF2 and ATF7 are dispensable for homeostatic turnover of the intestinal epithelium but are critically required to sustain sufficient epithelial repair after damage. ATF2 and ATF7 couple surface epithelial loss to a proportionate proliferative response and a decrease in secretory goblet cells providing an epithelial protective layer.

BACKGROUND & AIMS: Activation factor-1 transcription factor family members activating transcription factors 2 and 7 (ATF2 and ATF7) have highly redundant functions owing to highly homologous DNA binding sites. Their role in intestinal epithelial homeostasis and repair is unknown. Here, we assessed the role of these proteins in these conditions in an intestine-specific mouse model.

METHODS: We performed in vivo and ex vivo experiments using *Villin*-Cre^{ERT2}*Atf2*$^{fl/fl}$*Atf7*$^{ko/ko}$ mice. We investigated the effects of intestinal epithelium-specific deletion of the *Atf2* DNA binding region in *Atf7*$^{-/-}$ mice on cellular proliferation, differentiation, apoptosis, and epithelial barrier function under homeostatic conditions. Subsequently, we exposed mice to 2%

dextran sulfate sodium (DSS) for 7 days and 12 Gy whole-body irradiation and assessed the response to epithelial damage.

RESULTS: Activating phosphorylation of ATF2 and ATF7 was detected mainly in the crypts of the small intestine and the lower crypt region of the colonic epithelium. Under homeostatic conditions, no major phenotypic changes were detectable in the intestine of ATF mutant mice. However, on DSS exposure or whole-body irradiation, the intestinal epithelium showed a clearly impaired regenerative response. Mutant mice developed severe ulceration and inflammation associated with increased epithelial apoptosis on DSS exposure and were less able to regenerate colonic crypts on irradiation. In vitro, organoids derived from double-mutant epithelium had a growth disadvantage compared with wild-type organoids, impaired wound healing capacity in scratch assay, and increased sensitivity to tumor necrosis factor-α–induced damage.

CONCLUSIONS: ATF2 and ATF7 are dispensable for epithelial homeostasis, but are required to maintain epithelial regenerative capacity and protect against cell death during intestinal epithelial damage and repair. *(Cell Mol Gastroenterol Hepatol 2020;10:23–42; https://doi.org/10.1016/j.jcmgh.2020.01.005)*

Keywords: AP-1; DSS; TNF-α; Proliferation.

The intestinal epithelium allows the absorption of nutrients while at the same time providing the first line of defense against luminal threats such as noxious signals and pathogenic bacteria.[1] To support these essential functions, the intestinal epithelium is renewed rapidly and this process of renewal is tightly regulated by several mitogenic and morphogenic signaling pathways.[2] Intestinal epithelial stem cells reside at the bottom of so-called *crypts*, where they give rise to absorptive enterocytes[3] and secretory cells such as goblet cells, which secrete a protective mucus layer; hormone-secreting endocrine cells; and Paneth cells, which are unique to the small intestine.[4–6]

Several signaling pathways that regulate intestinal epithelial homeostasis and response to damage have been identified. Many of those belong to morphogenetic signaling families such as the Wnt (int/Wingless), Hedgehog, and bone morphogenetic protein families.[7] At the level of the epithelial cell these signals define cellular phenotype by tightly regulating the transcriptome through a set of key transcription factors.

Activating transcription factor 2 (ATF2) belongs to the large activation factor-1 (AP-1) transcription factor family. ATF2 can form homodimers as well as heterodimers with other AP-1 family members such as c-Jun. In intestinal homeostasis, inflammation, and cancer, the critical function of c-Jun has been studied extensively.[8–13] ATF2 is one of the potential heterodimer partners of c-Jun and is known to be regulated by pathways that play a critical role in the intestinal epithelium such as the Wnt and bone morphogenetic protein pathways.[14–18] Moreover, ATF2 contains an N-terminal activation domain that, as for c-Jun, can be activated by several mitogen-activated protein kinases (MAPKs), which have been implicated to play an important role in immune maintenance, hence regulating immune responses. For inflammatory bowel disease, mainly Crohn's disease, the importance of MAPKs p38 and c-Jun–N-terminal kinase have been described[19] and, additionally, a single-nucleotide polymorphism in the proposed ATF2-target gene *DMBT* was associated with Crohn's disease.[20] Despite these observations, the role of ATF2 in the intestinal epithelium has not yet been examined. Previous studies have shown that constitutive ATF2 knockout mice complete embryonic development, but die soon after birth owing to severe multiple organ deficiencies.[21–23] ATF2 has considerable sequence similarity to ATF7, both within the N-terminal activation domain and the DNA binding/dimerization domain.[24] Furthermore, the combination of ATF2 and ATF7 deficiency in mice leads to early embryonic defects, suggesting functional redundancy of these 2 factors.[22,24]

We hypothesized that ATF2 plays a key role in the intestinal epithelium, analogous to the importance of other AP-1 family members, such as c-Jun. By generating mice that carry an intestinal epithelial-specific deletion of the DNA binding domain of *Atf2* in a body-wide knockout of *Atf7*, we were able to examine the functional role of ATF2 and its highly homologous ATF7 in intestinal epithelial homeostasis and during damage and repair.

Results
Activated ATF2 Is Expressed Mainly in the Crypt Region of the Intestinal Epithelium

We first investigated the intestinal gene expression pattern of *Atf2* and *Atf7* in wild-type mice by quantitative reverse-transcription polymerase chain reaction (qRT-PCR). *Atf2* is expressed at similar levels in the colon and small intestine (Figure 1*A*), whereas expression of its close homolog *Atf7* is higher in the small intestine than in the colon (Figure 1*B*). Analysis by immunohistochemistry using an antibody that detects the transcriptionally active, phosphorylated form of both ATF2 and ATF7 showed that ATF2 and ATF7 localize to the crypt region of the small intestinal epithelium, where epithelial stem cells and Paneth cells reside. Expression of activated ATF2 and ATF7 was low in the villi, which contain differentiated cells (Figure 1*C*). Activated ATF2 and ATF7 followed a similar expression pattern for the colon, where the abundance gradually decreased from the bottom of the crypt toward the luminal side (Figure 1*D*).

ATF2 and ATF7 Are Not Required to Maintain Intestinal Epithelial Homeostasis

Because we detected expression of both ATF2 and ATF7 in the small intestine and colon, we decided to simultaneously delete both genes in the intestinal epithelium. Because whole-body deletion of *Atf2* is perinatally lethal but *Atf7* knockout mice have no apparent abnormalities, we crossed *Atf7* knockout mice with mice containing epithelial conditional deletion of *Atf2* DNA-binding domain ($Atf2^{floxed(fl)/floxed(fl)}$). To achieve this, we used mice with the intestinal epithelial-specific *Villin*-Cre$^{Estrogen\ Receptor\ 2\ (ERT2)}$, in which recombination can be induced by intraperitoneal injection of tamoxifen. *Villin*-Cre^{ERT2}*Atf2*$^{fl/fl}$ mice were crossed with mice with a constitutive knockout for the DNA binding domain (exon 10) of *Atf7*. *Villin*-Cre^{ERT2}*Atf2*$^{fl/fl}$ *Atf7*$^{wildtype(wt)/wildtype(wt)}$ control mice were compared with tamoxifen-induced *Villin*-Cre^{ERT2}*Atf2*$^{-/-}$*Aft7*$^{knockout(ko)/knockout(ko)}$ mice (henceforth referred to as $Atf2^{wt/wt}/7^{wt/wt}$ and $Atf2^{-/-}/7^{ko/ko}$, respectively). After recombination, mice were closely monitored and killed at 2 time points: 7 days and 60 days after recombination (Figure 2*A*). Knockout efficiency for *Atf2* and *Atf7* was confirmed by qRT-PCR. By using primers for the
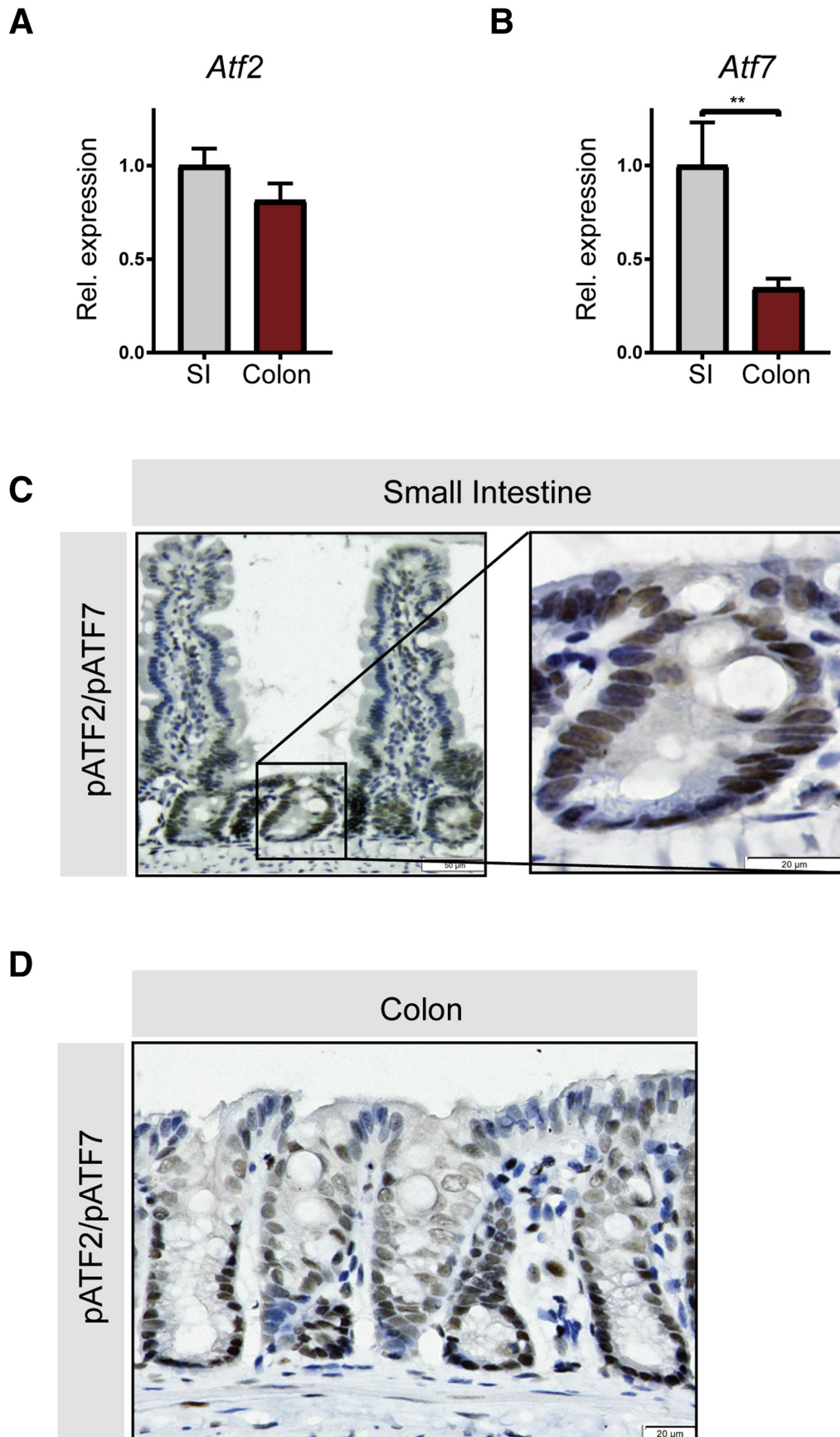
Most current article

A

Atf2

B

Atf7

C

Small Intestine

pATF2/pATF7

D

Colon

pATF2/pATF7

floxed exons on whole small intestinal and colon tissue, recombination was greater than 90% for both tissues (Figure 2B and C). $Atf2^{-/-}/7^{ko/ko}$ mice did not show any overall physical discomfort on recombination; nevertheless, the normal gain of body weight was reduced marginally after 60 days compared with $Atf2^{wt/wt}/7^{wt/wt}$ mice (Figure 2D), which has been observed previously in ATF7 mutant animals.[25] Histologic analysis by means of H&E staining of the small intestine and colon did not show any major phenotypic alterations for either 7 or 60 days after recombination. Crypt depth and villus length remained unaffected in the colon (Figure 2E, upper panel) and small intestine (Figure 2E, lower panel).

Because AP-1 transcription factors such as c-Jun are known to influence signaling pathways involved in cellular proliferation and differentiation, we next focused on examining the intestinal epithelial characteristics in $Atf2^{-/-}/7^{ko/ko}$ mice. No change was observed in the amount and localization of proliferative cells as determined by bromodeoxyuridine (BrdU) incorporation (Figure 3A–C). Furthermore, simultaneous deletion of $Atf2$ and $Atf7$ did not affect messenger RNA levels of stem cell marker $Lgr5$ (Figure 3D and E). Goblet cell differentiation was not affected as assessed by periodic acid–Schiff staining (Figure 3F–H) and markers of differentiated epithelial cells were not expressed differentially (Figure 3I and J). In conclusion, ATF2 and ATF7 are not essential for maintenance of proliferation and differentiation in adult intestinal tissues under homeostatic conditions.

ATF2 and ATF7 Are Required to Protect Against Epithelial Damage

ATF2 contains an N-terminal activation domain that can be activated by MAPKs.[23] For inflammatory bowel disease, mainly Crohn's disease, the importance of MAPKs, such as p38 and c-Jun-N-terminal kinase, has been reported.[19] Therefore, we addressed the question whether ATF2 and ATF7 play a role under stressed conditions. To achieve this, we used 2 models of inducing intestinal epithelial tissue injury. To damage the intestinal epithelium we exposed mice to a cycle of dextran sulfate sodium (DSS)[26] exposure and to whole-body ionizing radiation (IR). We first examined whether tissue injury and inflammation are influenced by the absence of functional ATF2 and ATF7 on exposure to DSS. $Atf2^{-/-}7^{ko/ko}$ and $Atf2^{wt/wt}7^{wt/wt}$ control mice were exposed to 2% DSS in drinking water for 7 consecutive days and killed 48 hours after the last DSS exposure (Figure 4A). $Atf2^{-/-}/7^{ko/ko}$ mice lost significantly more body weight (Figure 4B) and showed an increased disease activity score as indicated by the high colon density, edema, and visible blood, which are considered hallmarks of colitis (Figure 4C). Similarly, the histopathologic colitis activity score in $Atf2^{-/-}/7^{ko/ko}$ mice was significantly worse (Figure 4D) and mutant

mice developed significantly more ulceration relative to the colon length compared to wildtype mice (Figure 4E and F). Quantification of cytokines present in colon lysates reflected the worsened colitis in the $Atf2^{-/-}/7^{ko/ko}$ mice. Specifically, intestinal proinflammatory cytokine levels, such as tumor necrosis factor-α (TNF-α), interferon-γ, and interleukin 6 were increased significantly whereas levels of regulatory cytokines, such as interleukin 10, were unaltered (Figure 4G). These findings indicate that the simultaneous inactivation of $Atf2$ and $Atf7$ in the intestinal epithelium leads to increased sensitivity to DSS-induced colitis.

Next, we treated $Atf2^{-/-}/7^{ko/ko}$ and $Atf2^{wt/wt}/7^{wt/wt}$ control mice with 12 Gy whole-body IR, a sufficient dose to sensitize most of the stem cells in the small intestine.[27] At 24 hours after IR, massive apoptosis takes place of crypt epithelial cells followed by a cell-cycle arrest at 48 hours after irradiation. At approximately 96 hours after this initial epithelial damage, epithelial cells in the crypts start to hyperproliferate, resulting in hyperplastic crypts that undergo crypt fission to replace lost crypts and regenerate the epithelial layer. Therefore, we assessed the regenerative capacity of $Atf2^{-/-}/7^{ko/ko}$ epithelium at 96 hours after irradiation and focused our analyses on colonic tissue (Figure 5A). Histologic analysis by means of H&E staining showed a diminished regenerative response of $Atf2^{-/-}/7^{ko/ko}$ colonic crypts (Figure 5B). This notion was confirmed further by a significantly reduced amount of proliferative BrdU-positive cells (Figure 5C and D).

Finally, we performed an in vitro wound healing assay by introducing a scratch on a cell monolayer generated from primary colonic epithelial cells isolated from $Atf2^{-/-}/7^{ko/ko}$ and $Atf2^{wt/wt}/7^{wt/wt}$ control mice and capturing images of wound closing at a regular interval by a time-lapse microscope. Recombination of 2-dimensional (2D) cultures was confirmed by qRT-PCR at the $Atf2$ and $Atf7$ DNA binding locus. Analysis of wound closing upon mechanical damage showed reduced efficacy of ATF2- and ATF7-deficient colonic cells in closing the wound area (Figure 5E and F). Together these data indicate that ATF2 and ATF7 are critical mediators of intestinal repair after induced chemical, cytotoxic, and mechanical damage.

ATF2 and ATF7 Are Required to Protect Against Apoptosis and Maintain Goblet Cell Differentiation After DSS-Induced Colitis

We next focused on more careful analyses of the abnormalities that could underlie the aggravated response to DSS colitis in ATF2 and ATF7 mutant mice. In general, an increased sensitivity to DSS can be caused by reduced proliferative capacity of the intestinal epithelial cells, increased epithelial cell apoptosis, and/or impaired

---

Figure 1. (*See previous page*). **ATF2 and ATF7 are phosphorylated in proliferating colonic and small intestinal epithelial cells.** Small intestine (SI) and colon from wild-type C57BL/6 mice were analyzed for ATF2 and ATF7 localization. qRT-PCR for (*A*) $Atf2$ and (*B*) $Atf7$ in small intestine and colon tissue. (*C*) Immunohistochemistry for phospho-ATF2 and phospho-ATF7 in the small intestine (*left panel*), magnification of the crypt region in the small intestine (*right panel*). (*D*) Immunohistochemistry for phospho-ATF2 and phospho-ATF7 in colon tissue. (*A* and *B*) Ten mice per group were analyzed, graphs show means and SEM. **$P < .01$, Student t test. Rel., relative.
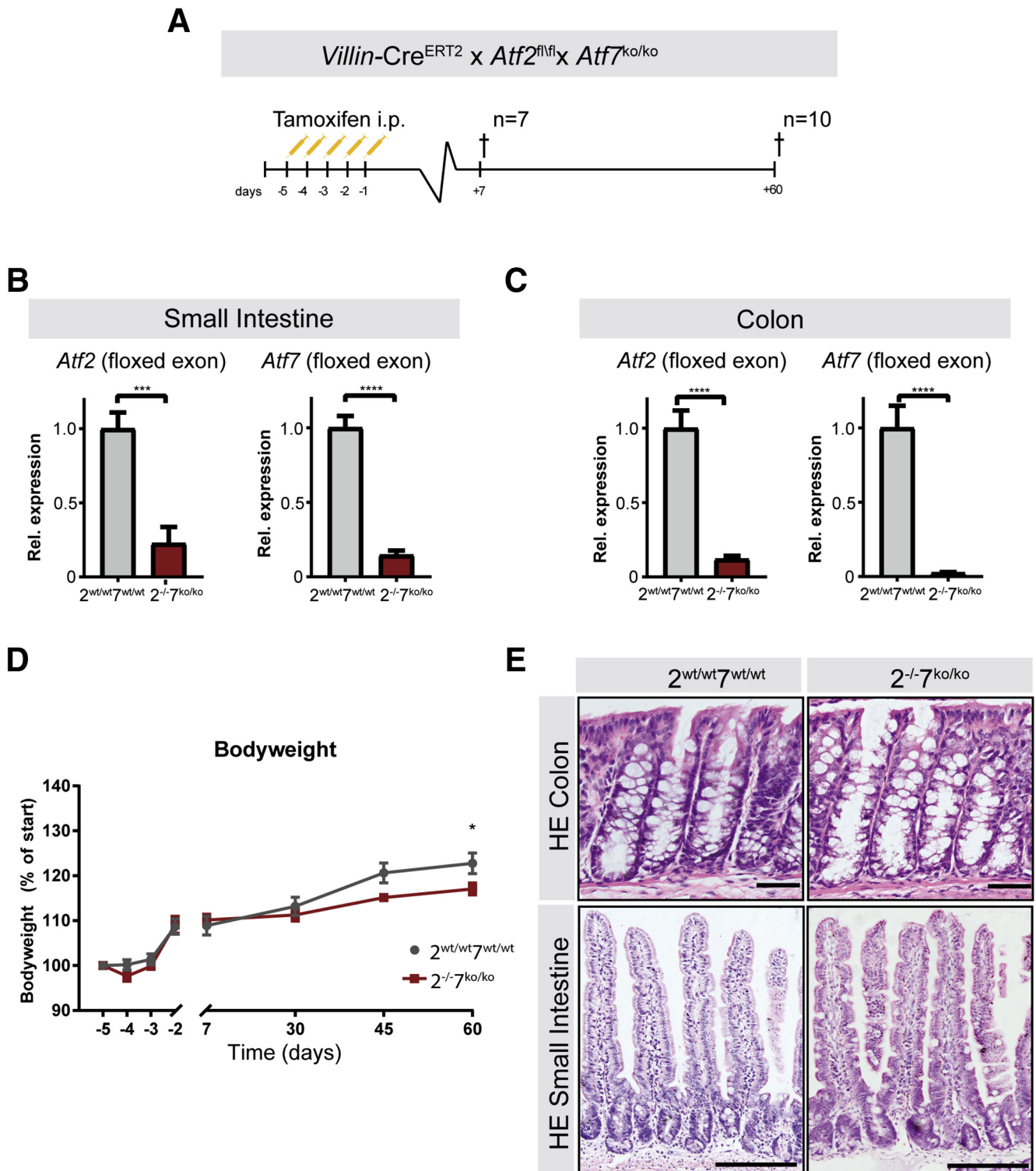
Figure 2. Deletion of intestinal ATF2 in ATF7 mutant mice. (*A*) *VillinCre^ERT2^Atf2^fl/fl^Atf7^+/+^* (*2^wt/wt^7^+/+^*) controls and *Villin-Cre^ERT2^Atf2^-/-^Atf7^ko/ko^* (*2^-/-^/7^ko/ko^*) mutant mice were injected intraperitoneally with 1 mg tamoxifen for 5 consecutive days. Mice were killed (†) 7 days (n = 7 per group) or 60 days (n = 10 per group) after the last tamoxifen injection. (*B* and *C*) qRT-PCR of the floxed exons of *Atf2* (*left panel*) and *Atf7* (*right panel*) on (*B*) whole small intestinal and (*C*) whole colon tissue at 60 days. (*D*) Body weight relative to the start of tamoxifen injections. (*E*) Representative images of H&E-stained sections of the colon in *Atf2^wt/wt^Atf7^+/+^* mice (*upper left*) and *Atf2^-/-^Atf7^ko/ko^* mice (*upper right*), and small intestine in *Atf2^wt/wt^Atf7^+/+^* mice (*lower left*) and *Atf2^-/-^Atf7^ko/ko^* mice (*lower right*). *Scale bars*: 50 μm. (*B–D*) n =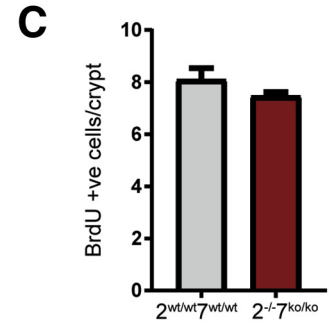 10 mice per group. (*B* and *C*) Graph bars show means and SEM. *$P < .05$, ***$P < .001$, and ****$P < .0001$, Student *t* test, and (*D*) Mann–Whitney per time point. HE, hematoxylin-eosin; Rel., relative.
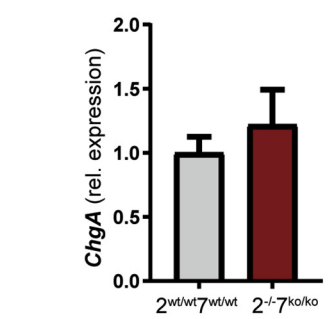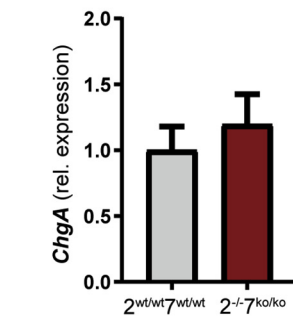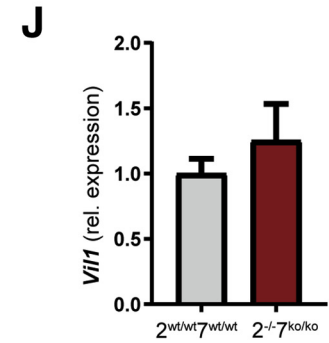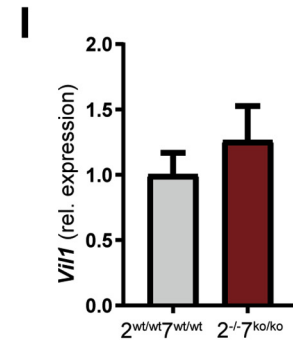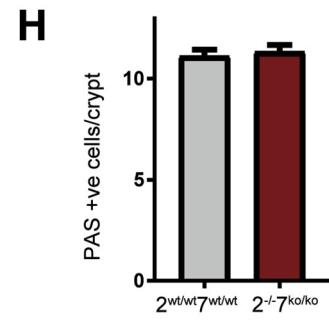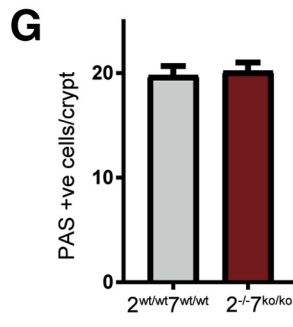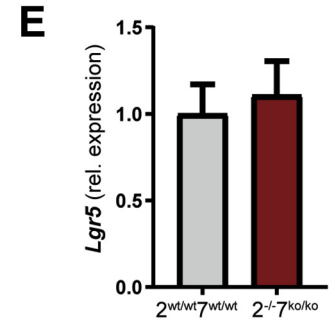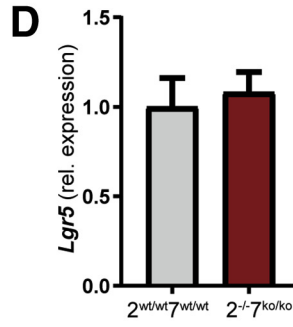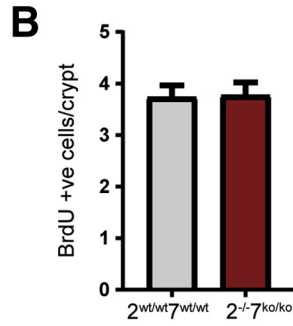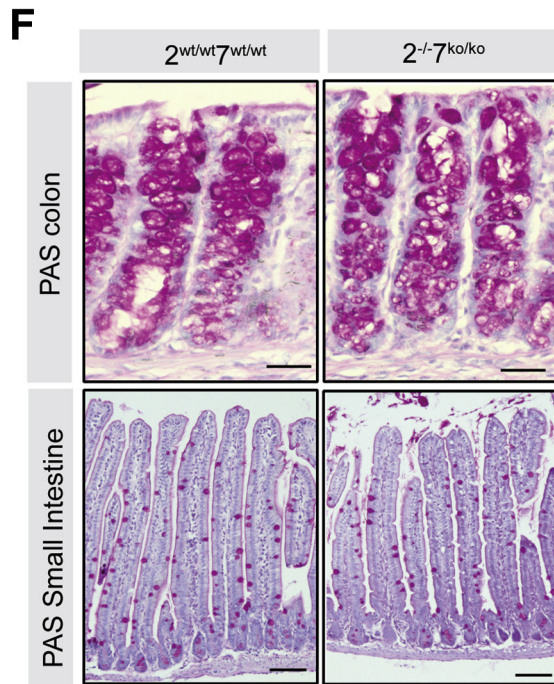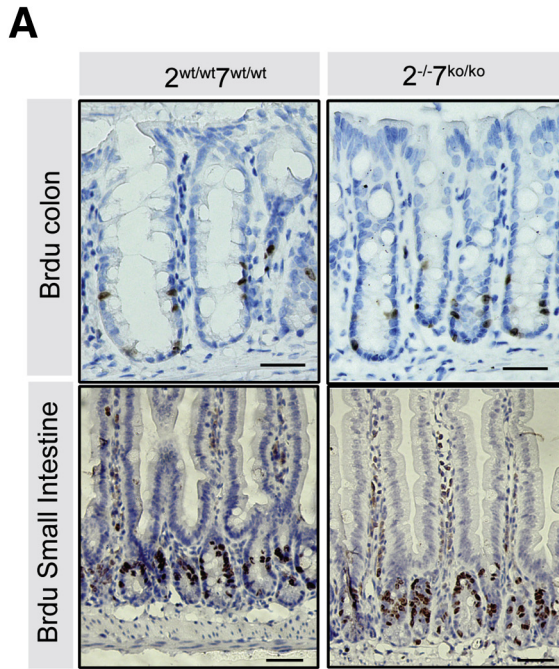
intestinal epithelial barrier function. To determine which of these processes are responsible for the aggravated colitis in $Atf2^{-/-}/7^{ko/ko}$ mice, we investigated the proliferative capacity of the intestinal epithelium after DSS administration. In healthy mice the intestinal epithelium responds to pathogenic stimuli by expansion and regeneration of the epithelium. This regeneration is fueled by either surviving leucine-rich-repeat-containing G-protein–coupled receptor 5 (Lgr5+) intestinal stem cells or other mature cell types such as secretory or absorptive committed progenitors of differentiated cell types able to convert back to Lgr5+ intestinal stem cells to aid in epithelial repair.[28] Under homeostatic conditions, the proliferation rate of epithelial cells, as assessed by BrdU incorporation, was not altered (Figure 3A and B). In DSS-exposed animals, epithelial proliferation was increased in the colonic crypts compared with homeostatic conditions, however, we did not observe any difference between control and $Atf2^{-/-}/7^{ko/ko}$ mice (Figures 3A and B compared with 6A and B, respectively). Interestingly, qRT-PCR analysis on colonic epithelial fractions showed a significant reduction of stem cell markers $Cd44$, $Lgr5$, and $Ascl2$ in the $Atf2^{-/-}/7^{ko/ko}$ mice after DSS (Figure 6C), indicating a reduced stem cell compartment. Indeed, quantification of $Lgr5$ transcripts confirmed this reduction (Figure 6D and E). In addition to the stem cell compartment, the differentiated cells seemed to be affected in $Atf2^{-/-}/7^{ko/ko}$ mice. Goblet cells play an important role in defense against pathogenic luminal signals and their numbers are relatively depleted during DSS colitis (Figure 1D compared with 3G). Importantly, in $Atf2^{-/-}/7^{ko/ko}$ mice the number of goblet cells was reduced further (Figure 6F and G). This correlated with a decrease of goblet and enteroendocrine cell markers $Muc2$ and $ChgA$ expression in the epithelial fractions (Figure 6H). Finally, we assessed the amount of epithelial cell apoptosis in the normal colon and in the DSS colitis model. The terminal deoxynucleotidyl transferase–mediated deoxyuridine triphosphate nick-end labeling (TUNEL) assay, which specifically marks apoptotic cells, showed increased apoptosis in $Atf2^{-/-}/7^{ko/ko}$ mice during DSS colitis (Figure 6I and J). In conclusion, $Atf2^{-/-}/7^{ko/ko}$ mice express reduced stem cell markers and goblet cell numbers while showing increased apoptosis in a model of DSS-induced epithelial damage.

Recombinant TNF-α Reduces Viability of ATF2- and ATF7-Deficient Colonic Epithelium In Vitro

TNF-α plays a pleiotropic role in the intestinal mucosa with both protective and proapoptotic effects. We hypothesized that epithelial cells in $Atf2^{-/-}/7^{ko/ko}$ mice are more sensitive to the proapoptotic epithelial effects of TNF-α and other proapoptotic mediators that are released during inflammation and that such sensitivity could play an important role in increased susceptibility to DSS colitis in $Atf2^{-/-}Atf7^{ko/ko}$ mice. To investigate this hypothesis, we used colonic epithelial organoids. Recombination was monitored at the $Atf2$ and $Atf7$ DNA binding locus by qRT-PCR (Figure 7A). As expected, both $Atf2^{wt/wt}Atf7^{wt/wt}$ and $Atf2^{-/-}/7^{ko/ko}$ organoids were able to grow and could be stably cultured for multiple passages. However, we observed that growth and size of $Atf2^{-/-}/7^{ko/ko}$ organoids was mildly restricted (Figure 7B and C). Remarkably, this growth retardation did not seem to rely on an altered proliferative capacity or reduced stemness because 5-Ethynyl-2′-deoxyuridine (EdU) incorporation and stem cell marker expression using qRT-PCR showed no change in $Atf2^{-/-}/7^{ko/ko}$ organoids compared with controls (Figure 7D and E). We next challenged the organoids with recombinant murine TNF-α. Organoids were reseeded and cultured for 3 days. Then, TNF-α was administered for 12 hours followed by 30 minutes of propidium iodide (PI) incubation to determine viability. Indeed, $Atf2^{-/-}/7^{ko/ko}$ organoids were more sensitive to TNF-α–induced cell death as assessed by microscopic analyses of viability (Figure 7F) and PI uptake (Figure 7G). These results suggest that the increased ulceration observed in $Atf2^{-/-}/7^{ko/ko}$ mice to DSS colitis can be attributed at least partially to increased epithelial sensitivity to apoptotic cell death.

TNF-α Induces Apoptotic and Inflammatory Pathways in ATF2- and ATF7-Deficient Background

To further examine the changes that underlie the increased sensitivity to apoptosis and impaired regenerative response observed in ATF2- and ATF7-deficient mice, we performed genome-wide expression analyses. We treated both colon organoids generated from $Atf2^{-/-}/7^{ko/ko}$ and control $Atf2^{wt/wt}/7^{wt/wt}$ mice with 50 ng/mL recombinant TNF-α for 12 hours. Principal component analyses of this multidimensional data set showed that although the global expression profile of unchallenged $Atf2^{wt/wt}/7^{wt/wt}$ and $Atf2^{-/-}/7^{ko/ko}$ was indistinguishable, the response to TNF-α treatment was distinct (Figure 8A). To assess the differences and similarities to the TNF-α response we performed a differential gene expression analysis. Of approximately 450 genes that were up-regulated ($P < .05$; fold change, >1.5) in colon organoids of both genotypes treated with recombined

---

Figure 3. (*See previous page*). **ATF2 and ATF7 are not required for proliferation, expression of stem cell markers, and epithelial differentiation under homeostatic conditions.** The experiment was performed as described in Figure 2. (*A*) Immunohistochemistry for BrdU at 60 days after recombination. *Upper panels*: colon (*scale bars*: 25 μm), *lower panels*: small intestine (*scale bars*: 100 μm). (*B* and *C*) Quantification of BrdU-positive cells per crypt in the (*B*) colon and (*C*) small intestine. (*D* and *E*) qRT-PCR for transit-amplifying/stem cell markers in the isolated (*D*) colonic and (*E*) small intestinal epithelial fraction. (*F*) Periodic acid–Schiff (PAS) staining 60 days after recombination: *upper panels*: colon (*scale bars*: 25 μm), *lower panels*: small intestine (*scale bars*: 100 μm). (*G* and *H*) Quantification of PAS-positive cells per crypt in the (*G*) colon and (*H*) small intestine. (*I* and *J*) qRT-PCR for differentiated cell compartment markers in (*I*) colon and (*J*) small intestine epithelial fractions. (*B–J*) n = 10 mice per group. Graph bars show means and SEM. Student *t* test. rel., relative.
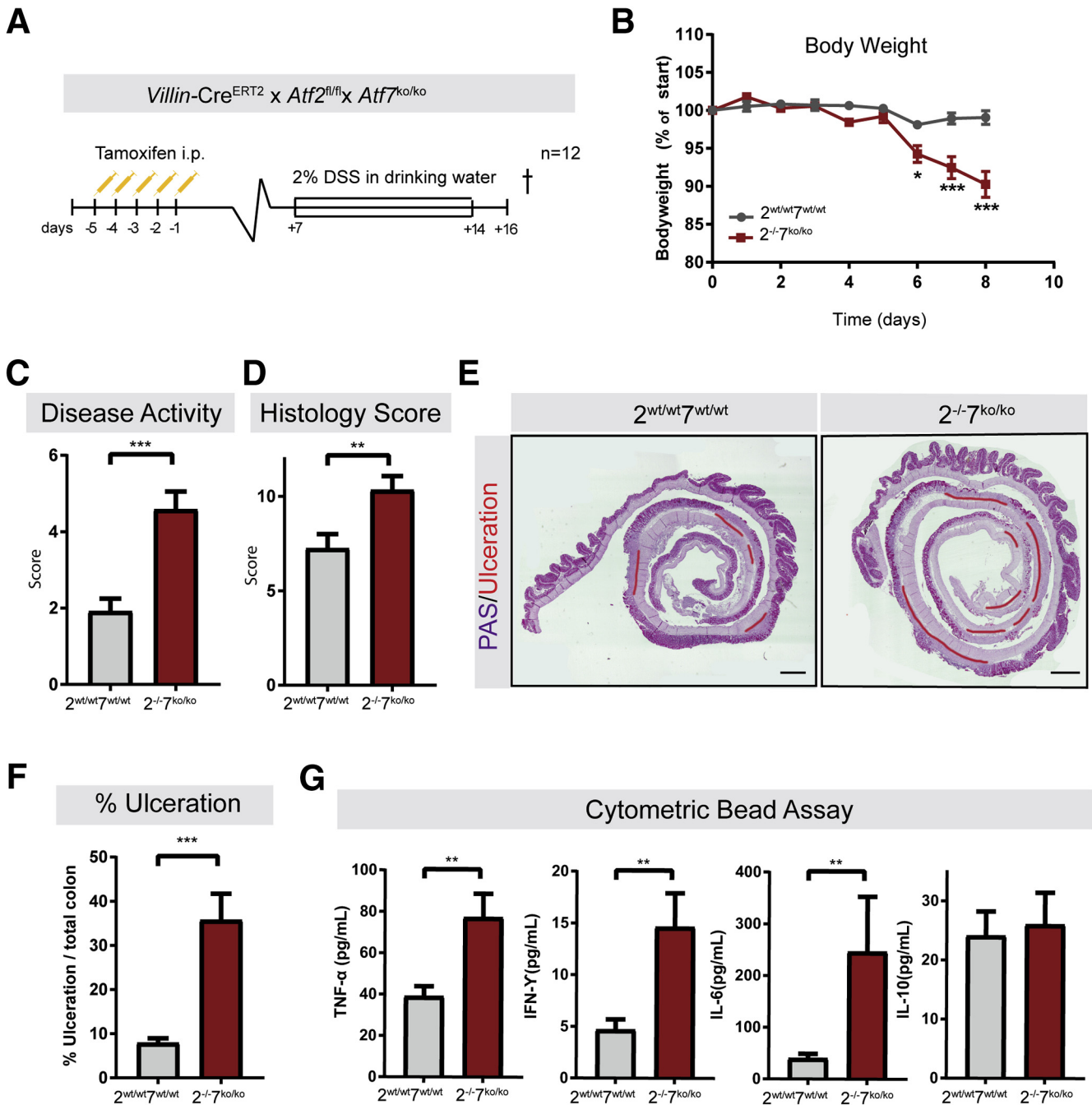
Figure 4. Depletion of intestinal ATF2 and ATF7 aggravates epithelial damage in response to 2% DSS. (*A*) *Villin*-Cre[ERT2]-*Atf2*[wt/wt]*Atf7*^{+/+} (n = 12) and *Villin*-Cre[ERT2]-*Atf2*^{fl/fl}*Atf7*[ko/ko] (n = 12) were injected intraperitoneally with 1 mg tamoxifen for 5 consecutive days. Animals were provided with drinking water containing 2% DSS for 7 days, starting 7 days after induction of recombination. Mice were killed (†) 2 days after the last DSS administration. (*B*) Body weight relative to start of DSS exposure. (*C*) Disease activity score. (*D*) Histopathology score. (*E*) Representative images of periodic acid–Schiff (PAS)-stained sections of the colons of a mutant mouse and control. Ulceration is highlighted in red. *Scale bar*: 750 μm. (*F*) Quantification of percentage of ulceration related to total colon length. (*G*) Protein levels of TNF-α, interferon (IFN)-γ, interleukin (IL)6, and IL10. (*B*–*G*) n = 12 mice per group. Graph bars show means and SEM. *P < .05, **P < .01, and ***P < .001, Student t test and (*B*) Mann–Whitney per each time point was performed.

TNF-α, 225 genes were in common between *Atf2*[wt/wt]/*7*[wt/wt] and *Atf2*^{-/-}/*7*[ko/ko]. However treatment with recombinant TNF-α induced a distinct response in *Atf2*^{-/-}/*7*[ko/ko]-deficient organoids that consisted of 99 genes significantly up-regulated on TNF-α treatment specifically. More detailed analysis of this response showed genes involved in inflammation such as *Il17* and *Il7*, and involved in apoptosis such as *Irak2*, *Blc10*, and *Parp* (Figure 8C). Gene ontology (GO)

A
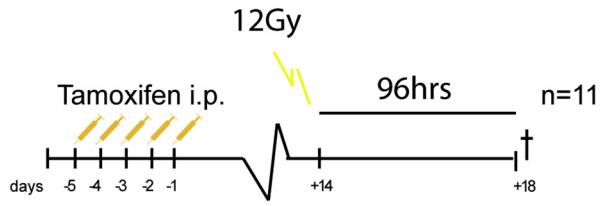
B
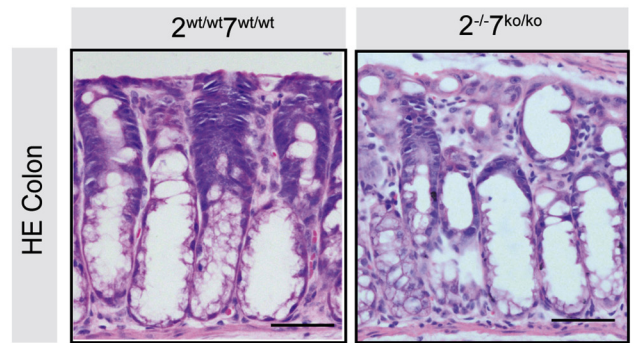
C
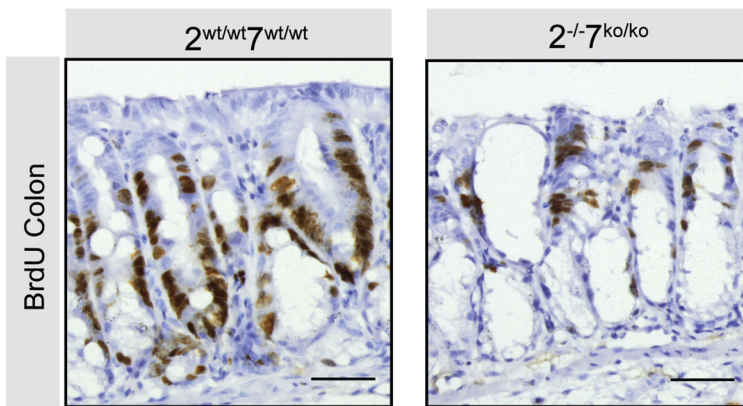
D
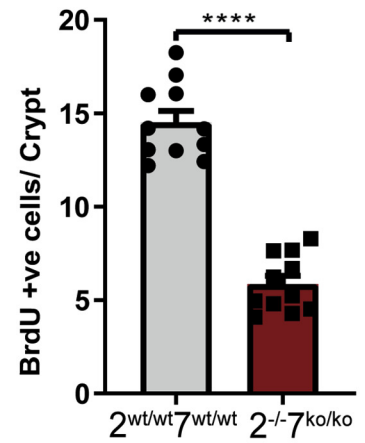
E
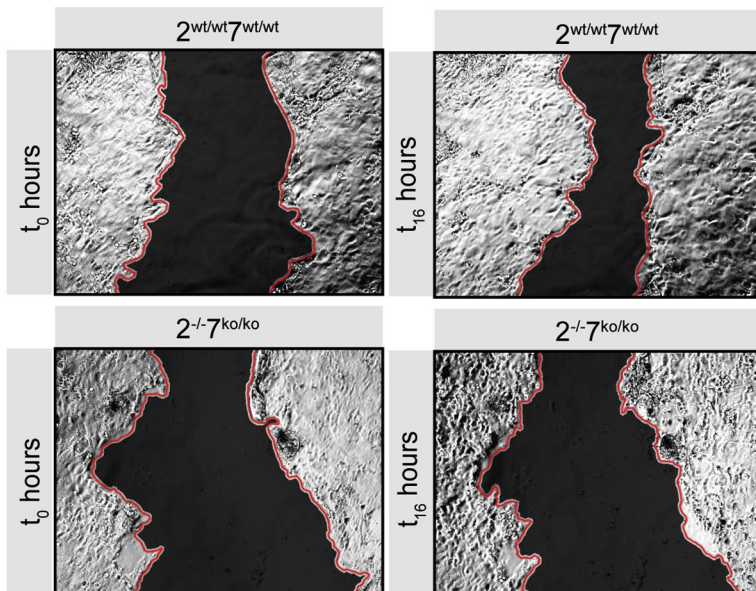
F
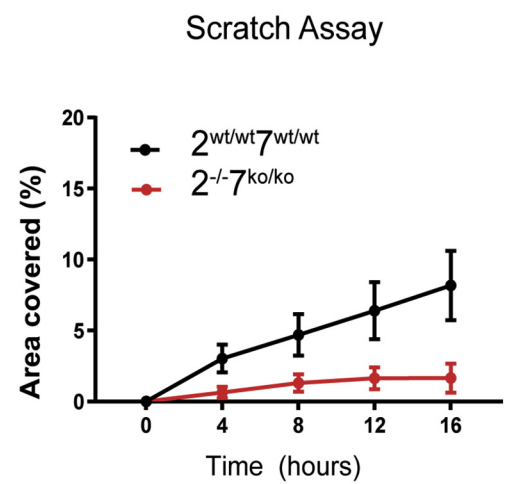
analysis of all differentially expressed genes between $Atf2^{wt/wt}/7^{wt/wt}$ and $Atf2^{-/-}/7^{ko/ko}$ colonic organoids showed predominant changes in canonical pathways related to the inflammatory response and brush-border membrane, which are important processes for sensitivity to DSS (Figure 8D).

Intestinal Barrier Function Is Not the Predisposing Factor for DSS Sensitivity in Atf2$^{-/-}$/7$^{ko/ko}$ mice

Because GO profiles identified brush-border membrane function as a significantly changed alteration between control and $Atf2^{-/-}/7^{ko/ko}$ organoids after TNF-α treatment, we decided to examine if ATF2 and ATF7 play a role in barrier function under homeostatic conditions. Such diminished barrier function could be an additional reason $Atf2^{-/-}/7^{ko/ko}$ mice would be predisposed to having more severe colitis. To examine this possibility, we performed a functional fluorescein isothiocyanate (FITC) dextran assay and assessed intestinal permeability in unchallenged mice (Figure 9A). After in vivo recombination, followed by a recovery phase, mice were fasted and subsequently orally gavaged with FITC dextran. Four hours after gavage, FITC serum levels were determined as a readout for intestinal permeability. Serum FITC levels were not different between the experimental groups, showing that there was no impairment of the intestinal barrier function in $Atf2^{-/-}/7^{ko/ko}$ mutant mice. Therefore, it is unlikely that reduced epithelial barrier function was a predisposing factor for the increased sensitivity to DSS-induced epithelial damage and colitis (Figure 9B). In support, no differences could be observed in the abundance of tight junction complex proteins zonula occludens-1 and E-cadherin, as assessed by immunostaining (Figure 9C and D). In addition, there was no change between $Atf2^{-/-}/7^{ko/ko}$ and control mice in gene expression levels of tight junction proteins (Figure 9E), as assessed by qRT-PCR, or in tight junction morphology, as assessed by electron microscopy (Figure 9F and G). These data suggest that there are no changes in intestinal epithelial barrier function after deletion of $Atf2$ and $Atf7$ in homeostatic conditions.

Discussion

In this study we show that the functionally homologous AP-1 transcription factors ATF2 and ATF7 are dispensable for homeostatic turnover of the intestinal epithelium but are critically required to sustain sufficient epithelial repair upon damage.

To investigate the role of ATF2 and ATF7 in the adult intestine, we used $Atf7$ mutant mice and crossed them with mice in which we could specifically induce deletion of the DNA binding domain of $Atf2$ in the intestinal epithelium. In contrast to the severe phenotype observed in $Atf2$ mutant mice during embryonic development,[22,24] intestinal epithelial deletion of ATF2 and ATF7 did not lead to an overt phenotype in the unchallenged adult intestine. However, upon DSS-induced epithelial injury and irradiation, these mice showed substantially increased colonic ulceration and reduced regenerative capacity, respectively.

The intestinal epithelium is a highly regenerative tissue that is able to overcome damage after an insult through several adaptive mechanisms such as a rapid induction of epithelial proliferation after loss of surface epithelial cells, the protection of epithelial cells against apoptosis, efficient closure of the wounded surface area, and a well-balanced inflammatory response that resolves as the epithelial barrier is restored without turning the original insult into a chronic inflammatory state.[29,30] The aggravated epithelial damage on exposure to a damaging agent such as DSS and whole-body irradiation in the $Atf2^{-/-}/7^{ko/ko}$ animals was associated with substantially increased epithelial damage and decreased regenerative capacity, respectively. This suggested that ATF2 and ATF7 may be required to protect the intestinal epithelium from excessive cell death during damage and ensure adequate epithelial repair. Indeed, when we cultured $Atf2$ and $Atf7$ double-mutant epithelial cells in vitro in organoid cultures, we observed enhanced sensitivity to recombinant TNF-α–mediated cell death. Gene array analysis showed that genes associated with inflammatory and apoptotic responses were among up-regulated genes in response to TNF-α treatment, specifically in the $Atf2^{-/-}/7^{ko/ko}$ background. Interestingly, GO analysis identified brush-border membrane alterations among the most significantly changed GO terms between control and $Atf2^{-/-}/7^{ko/ko}$ organoids after TNF-α treatment. This suggested that ATF2 and ATF7 deficiency might have an effect on tight junction complexes, hence predisposing $Atf^{-/-}Atf7^{ko/ko}$ mice to more severe colitis. However, we found no evidence to support this hypothesis.

Mice that have a body-wide deletion of both $Atf2$ and $Atf7$ do not survive embryogenesis because of severe developmental abnormalities in the liver and heart.[24] It was

Figure 5. (*See previous page*). **ATF2 and ATF7 are required for appropriate epithelial repair upon damage.** (*A*) *Villin*-Cre^{ERT2}-$Atf2^{wt/wt}Atf7^{+/+}$ (n = 11) and *Villin*-Cre^{ERT2}-$Atf2^{fl/fl}Atf7^{ko/ko}$ (n = 11) were injected intraperitoneally with 1 mg tamoxifen for 5 consecutive days. Fourteen days after induction of recombination mice were irradiated with 12 Gy and killed (†) 96 hours after irradiation. (*B*) Representative images of H&E immunohistochemistry of irradiated colons 96 hours after irradiation. *Scale bars*: 50 μm. (*C*) Representative images of immunohistochemistry for BrdU in colons of irradiated mutant and control animals. *Scale bars*: 50 μm. (*D*) Quantification of BrdU-positive cells in colonic crypts. n = 11 mice per group. (*E*) Representative images of scratch wound assay of $Atf2^{wt/wt}Atf7^{+/+}$ (*left panels*) and $Atf2^{-/-}Atf7^{ko/ko}$ (*right panels*) cell monolayers at 0 hours (*left panels*) and 16 hours (*right panels*) after scratching. Wounds artificially have been colored black and the scratch edges colored red to aid visualization. (*F*) Representative experiment showing SEM based on measuring the area of 8 fields of the wound per condition. The experiment was repeated 3 independent times with similar results. The area of the wound (shown in panel *E*) covered by $Atf2^{fl/fl}Atf7^{+/+}$ (*black circles*) and $Atf2^{-/-}Atf7^{ko/ko}$ (*red circles*) was measured every 2 hours and quantified with ImageJ. n = 3 independent experiments. Graph bars show means and SEM. ****P < .0001, Student t test. HE, hematoxylin-eosin.
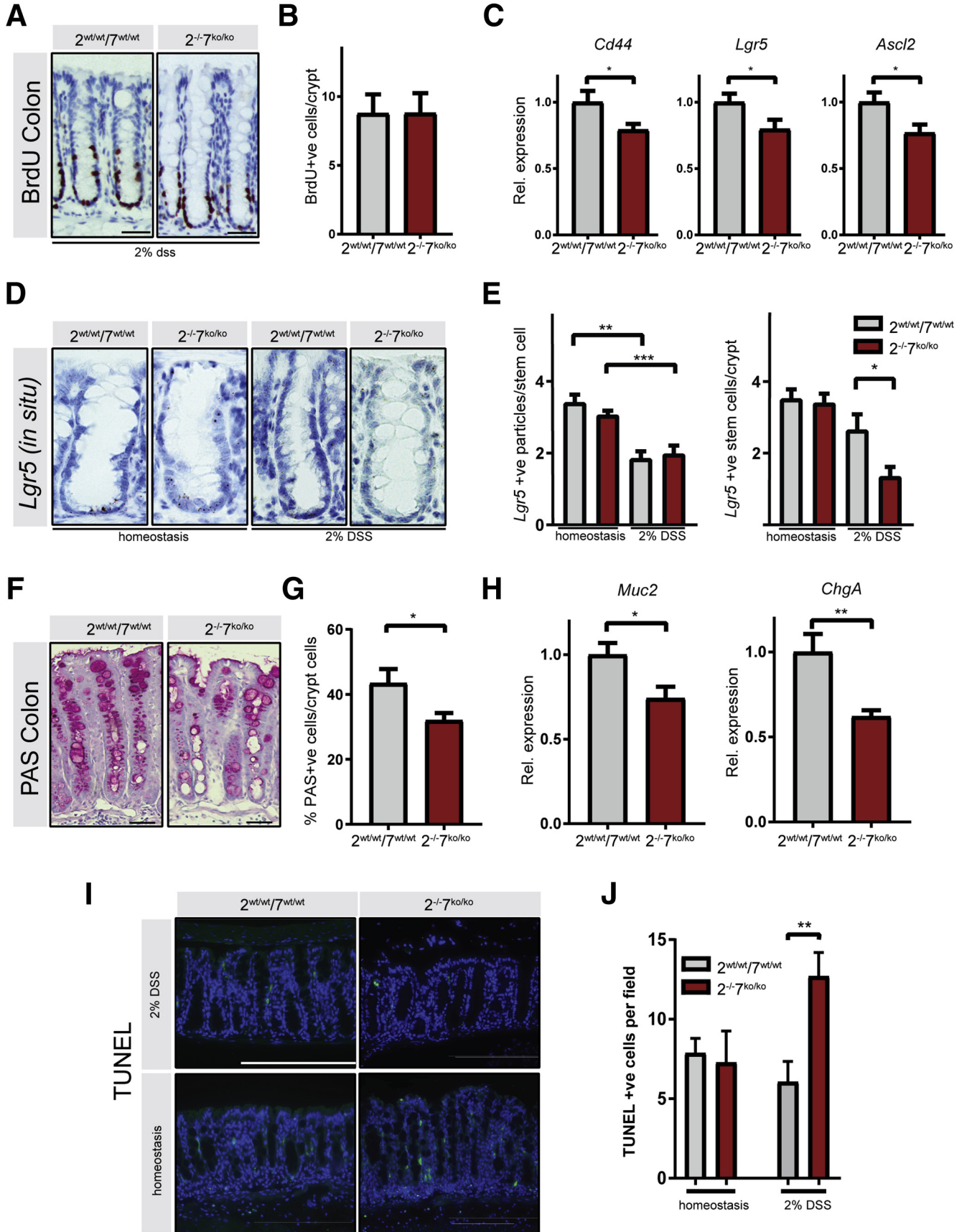
found that the liver abnormalities result from increased hepatocyte apoptosis caused by excess p38 MAPK activation. In addition, ATF2 is required for the transcriptional regulation of MAPK phosphatases that are required to limit p38 MAPK activation.[31] We examined p38 MAPK phosphorylation in our mutant mice, but did not observe any noticeable difference between wild-type and mutant animals (data not shown). In support of this, we find no evidence for altered MAPK pathway genes from global expression analyses after combined ATF2 and ATF7 deletion.

The excess epithelial apoptosis in mutant animals was coupled to an epithelial proliferative response that was comparable with control animals. Of note, although the rate of proliferation was similar between mutant animals and controls, this suggests that the proliferative response was not able to compensate for the increased rate of apoptosis in mutant animals, which suggests a relatively diminished capacity for epithelial regeneration in addition to the excessive apoptosis. This could fit well with the reduced expression of stem cell markers *Lrg5* and *Ascl2* observed in mutant animals in vivo. In addition to the impaired response to epithelial damage after a challenge with DSS, we observed a similar defective regenerative response after irradiation in vivo and when culturing mutant organoids in vitro. When we cultured *Atf2* and *Atf7* double-mutant organoids in vitro, they consistently showed a mild growth retardation compared with wild-type organoids. This corresponds to the fact that the epithelium in organoid culture is not in a state of homeostasis but constantly expanding and therefore thought to be more reflective of a situation of epithelial repair.[32,33] In addition, when culturing the epithelial cells in a 2D structure, $Atf^{-/-}Atf7^{ko/ko}$ organoids showed impaired epithelial regeneration upon mechanical damage.

An additional factor that may have contributed to the severe inflammation in *Atf2* and *Atf7* mutant animals is the inability to sustain the appropriate generation of goblet cells. Goblet cells are the source of the highly glycosylated mucin 2, which forms the protective intestinal mucus layer. The key role of mucin 2 in protection against epithelial damage is evident from the fact that *mucin 2* mutant animals spontaneously develop colitis.[34] Unfortunately, whether the

increased loss of goblet cells shown in $Atf^{-/-}Atf7^{ko/ko}$ mice is a cause or consequence of the increased epithelial damage upon DSS treatment was not elucidated in our experiments.

Together our observations suggest that ATF2 and ATF7 are required to protect the epithelial layer against excessive damage upon damaging stimuli, and couple surface epithelial loss to a proportionate proliferative response and a decrease in secretory goblet cells providing an epithelial protective layer.
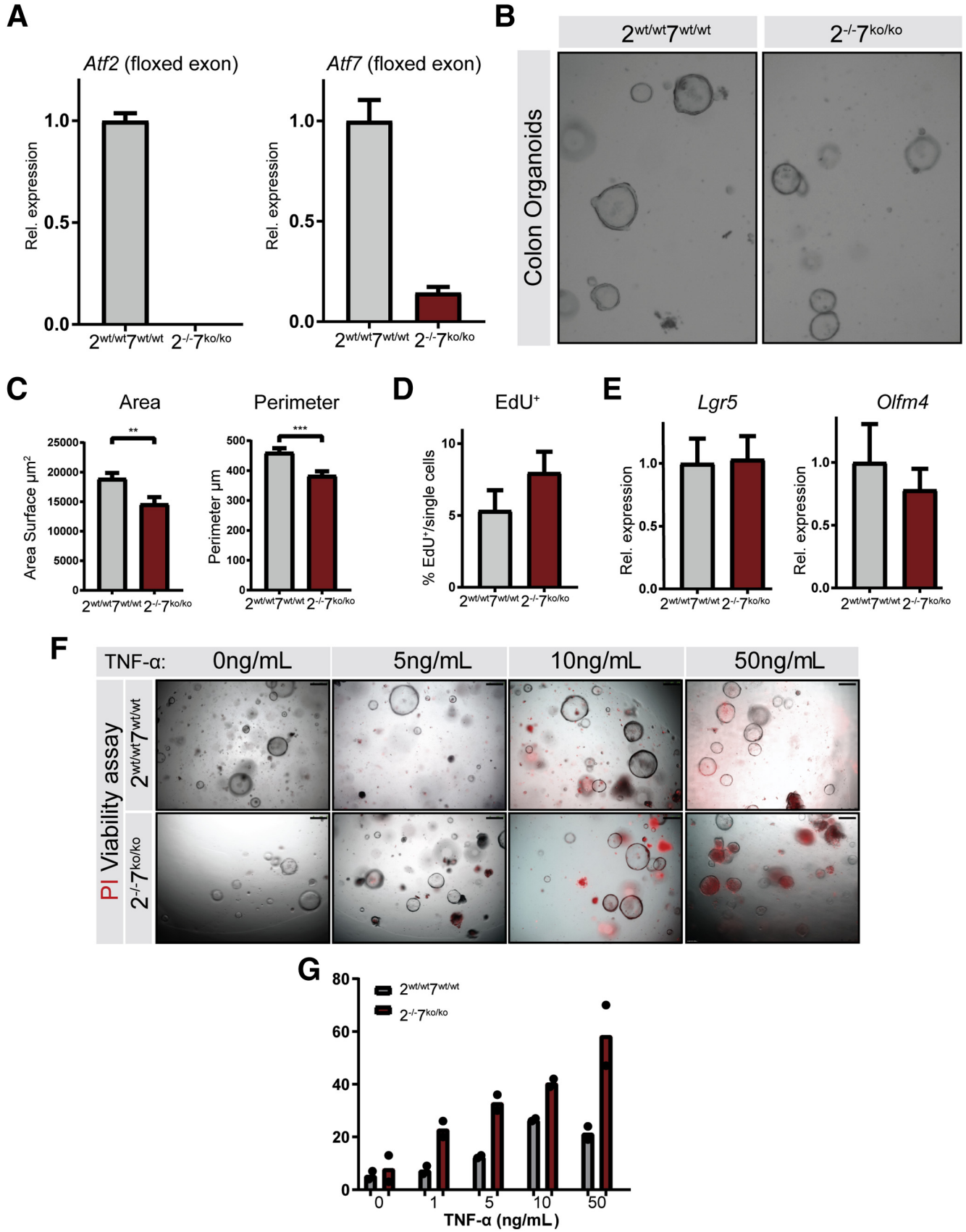
Material and Methods
Animals

For all experiments, C57BL/6, *Villin-CreERT2* mice[35] were crossed with $Atf2^{fl/fl}$-$Atf7^{ko/ko}$[24] mice to generate *Villin-CreERT2-* $Atf2^{fl/fl}$-$Atf7^{ko/ko}$ animals. All animals were housed at the Animal Research Institute of the Academic Medical Center Amsterdam. All experiments were approved by the relevant local ethical committees. Activation of CreERT2 and thus induction of the respective gene manipulations was performed by intraperitoneal administration of 1 mg tamoxifen (Sigma-Aldrich, St. Louis, MO) for 5 consecutive days. Mice were killed on day 7 (n = 7) and day 60 (n = 10) after recombination. Body weights were measured repeatedly. Small intestine and colon were removed from mice, flushed with cold phosphate-buffered saline (PBS), opened longitudinally, and fixed in 4% formaldehyde solution. Colons were fixed as Swiss rolls. Before fixation, the length and weight of small intestine and colon was determined.

Colitis Induction

Drinking water was supplemented with 2% DSS (Sigma Aldrich) for 7 days, followed by 2 days of regular drinking water. Mice (n = 12 per group) were killed 9 days after initial DSS administration, with intraperitoneal BrdU administration 2 hours before killing. Body weights were measured daily during DSS administration. Water consumption was monitored by eye per cage. Water bottles were filled daily with 50 mL DSS-H_2O and checked for volume every refreshment. We did not observe differences between both study groups when corrected for

Figure 6. (*See previous page*). **ATF2 and ATF7 are required to prevent apoptosis and sustain goblet cell differentiation after DSS-induced damage.** The experiment was performed as described in Figure 4*A*. (*A*) Representative images of immunohistochemistry for BrdU in colons of DSS-treated mutant and control animals. *Scale bar*: 750 μm. (*B*) Quantification of BrdU-positive cells in intact colonic crypts. (*C*) qRT-PCR of the isolated epithelial fraction for epithelial stem cell markers *Cd44*, *Lgr5*, and *Ascl2*. (*D*) Representative images of colonic RNA scope in situ hybridization for *Lgr5* messenger RNA in homeostasis (as described in Figure 1*A*) and on exposure to 2% DSS. (*E*) quantification of *Lgr5* messenger RNA particles per colonic Lgr5-positive stem cell (*left panel*) and quantification of *Lgr5*-positive cells per colonic crypt (*right panel*). Mice were analyzed for homeostasis: $Atf2^{wt/wt}Atf7^{+/+}$ (n = 8) and $Atf2^{-/-}Atf7^{ko/ko}$ (n = 8), and for 2% DSS: $Atf2^{wt/wt}Atf7^{+/+}$ (n = 4) and $Atf2^{-/-}Atf7^{ko/ko}$ (n = 4). (*F*) Representative immunohistochemistry image of colonic periodic acid–Schiff (PAS) staining. (*G*) Relative abundance of PAS-positive cells per crypt epithelial cells. (*H*) qRT-PCR for secretory epithelial markers in isolated colonic epithelial fraction. (*I*) TUNEL staining (green) with 4′,6-diamidino-2-phenylindole counterstain (blue). *Upper panels*: colons from mice not treated with DSS (n = 5 per group). *Lower panels*: colons from mice treated with DSS for 7 days (n = 6 mice per group). *Scale bar*: 600 μm. (*J*) Quantification of TUNEL-positive cells per microscopic field (5 random fields per mouse). Mice were analyzed for homeostasis: $Atf2^{wt/wt}Atf7^{+/+}$ (n = 5) and $Atf2^{-/-}Atf7^{ko/ko}$ (n = 5), and for 2% DSS: $Atf2^{wt/wt}Atf7^{+/+}$ (n = 6) and $Atf2^{-/-}Atf7^{ko/ko}$ (n = 6). (*B*, *C*, *G*, and *H*) n = 12 mice per group. Graph bars show means and SEM. *$P < .05$, **$P < .01$, ***$P < .001$, Student *t* test for panels *B*, *C*, *G*, and *H*, 1-way analysis of variance test for panels *E* and *J* followed by the Bonferroni test for selected groups. Rel., relative.

A

Atf2 (floxed exon)

Atf7 (floxed exon)

B Colon Organoids

C Area | Perimeter

D EdU⁺

E *Lgr5* | *Olfm4*

F TNF-α: 0ng/mL | 5ng/mL | 10ng/mL | 50ng/mL

PI Viability assay

G TNF-α (ng/mL)

mouse per cage, intake was approximately 3–4 mL per mouse (3 or 4 mice per cage). Colons were removed from mice, scored for the presence of feces and blood, flushed with ice-cold PBS, opened longitudinally, and fixed in 4% formaldehyde solution. Colons were fixed as Swiss rolls. Before fixation, colon length and weight were determined. A standardized scoring system was used to assess the severity of colitis both clinically and histopathologically.[36] Table 1 shows a detailed description of the scoring system.

Irradiation

Mice were irradiated with 12 Gy (n = 11 per group), 14 days after tamoxifen recombination. Ninety-six hours after irradiation mice were killed with intraperitoneal BrdU administration 2 hours before death. Colons were removed from mice flushed with ice-cold PBS, opened longitudinally, and fixed in 4% formaldehyde solution. Colons were fixed as Swiss rolls and analyzed for proliferation by means of BrdU incorporation.

Measurement of Intestinal Permeability

To determine intestinal permeability in vivo, mice were starved for 6 hours and FITC dextran (FD4; Sigma-Aldrich, St. Louis, MO) was administered by oral gavage (44 mg/100 g body weight). After 4 hours, mice were killed and blood was collected by cardiac puncture. Serum was separated from whole blood using BD Microtainer SST Tubes (365968; BD Biosciences, San Jose, CA), diluted with an equal volume of PBS (pH 7.4), and 100 mL of diluted serum was added to a black 96-well microplate. The concentration of FITC in serum was determined by spectrophotofluorometry, with an excitation of 485 nm and an emission wavelength of 528 nm, using serially diluted FITC dextran as standard.

Immunohistochemistry

Tissue was fixed in 4% ice-cold formalin and embedded in paraffin. Sections of 4-μm thickness were deparaffinized in xylene and rehydrated. Endogenous peroxidase was blocked using 0.3% H_2O_2 in methanol for 30 minutes. The following methods of antigen retrieval were used: sodium citrate (slides were cooked at 100°C for 20 minutes in 0.01 mol/L sodium citrate, pH 6); Tris/EDTA (slides were cooked at 100°C for 20 minutes in a Tris/EDTA buffer, 10 mmol/L Tris, 1 mmol/L EDTA, pH 9.0); and proteinase K (slides were incubated with proteinase K [S302030; Dako, Santa Clara, CA] for 5 minutes at room temperature). After antigen retrieval, slides were blocked in phosphate buffered saline (PBS) with 1% bovine serum albumin (BSA) and 0.1% Triton X-100 (Sigma-Aldrich) (PBS/BSA/Triton [PBT]) for 30 minutes, followed by incubation overnight at 4°C with a primary antibody in PBT. The following antibodies were used: pATF2/7 (9221S, 1:500, Cell Signaling Technology, Beverly, MA), anti-BrdU BMC9318 (1:500; Roche, Basel, Switzerland), E-cadherin (610181; BD Biosciences), and zonula occludens-1 (Invitrogen, Waltham, MA40-2200; 1:1000). Antibody binding was visualized using Powervision horseradish-peroxidase–labeled secondary antibodies from Immunologic (Duiven, the Netherlands) or biotinylated anti-rat (E0468; Dako) and streptavidin/horseradish-peroxidase (P039701; Dako) and diaminobenzidine (Sigma-Aldrich) for substrate development. All sections were counterstained with Mayer's hematoxylin.

For immunofluorescence, slides were incubated for 1 hour using fluorescently labeled secondary antibodies (all Alexa Fluor secondary antibodies were from Invitrogen, Waltham, MA), diluted 1:500 in PBS with 0.1% Triton X-100 and 1% bovine serum albumin at room temperature. Slides were washed and mounted with Slowfade Gold Antifade reagent with 4′,6-diamidino-2-phenylindole (s36938; Invitrogen). Images were obtained on a Leica DM6000 Digital Microscope equipped with LAS AF Software (Leica, Wetzler, Germany). For analysis, the software program ImageJ (available from: www.rsbweb.nih.gov/ij; National Institutes of Health, Bethesda, MD) was used.

RNAscope in situ hybridization was performed according to the manufacturer's protocol (Advanced Cell Diagnostics Segrate, Milano, Italy). The single-plex RNAscope probes against mouse *Lgr5* (312171; Advanced Cell Diagnostics) were used.
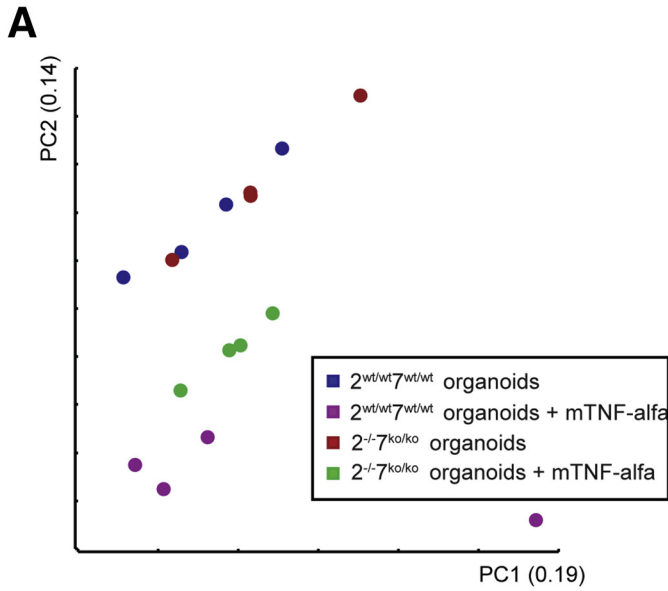
TUNEL Assay

Apoptosis was detected in paraffin-embedded colon samples using the Fluorescein In Situ Cell Death Detection Kit (Roche) according to the manufacturer's instructions. Images were taken with a Leica DM6000 Digital Microscope equipped with LAS AF Software (Leica), using appropriate fluorescence filters. Positive TUNEL cells were counted per microscopic field.
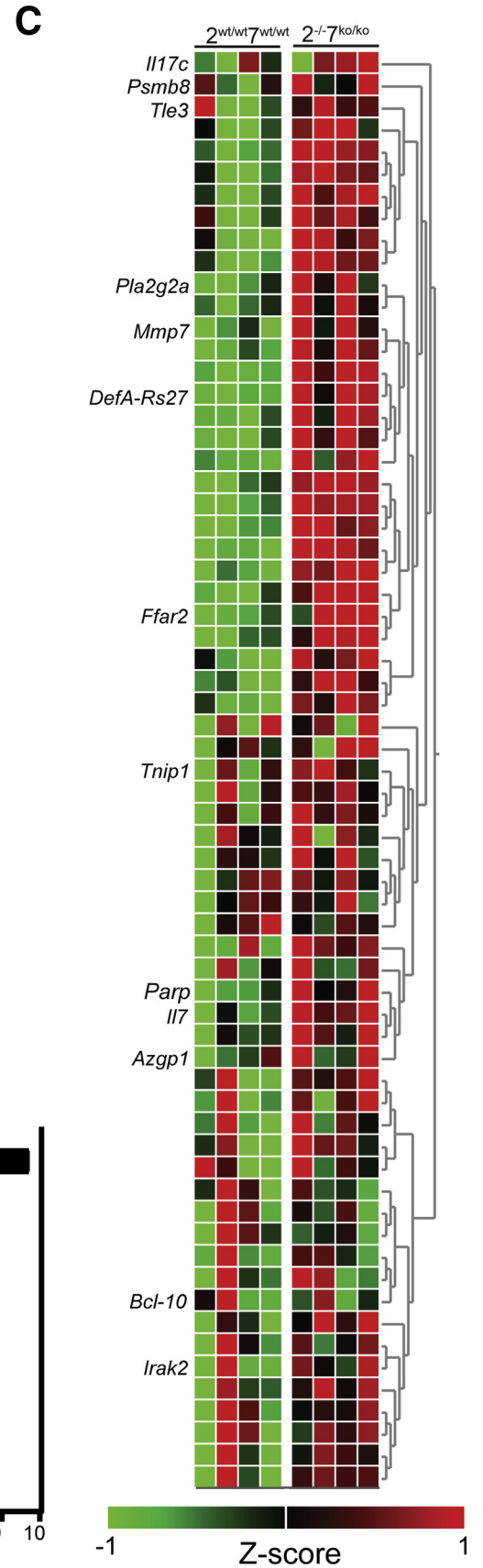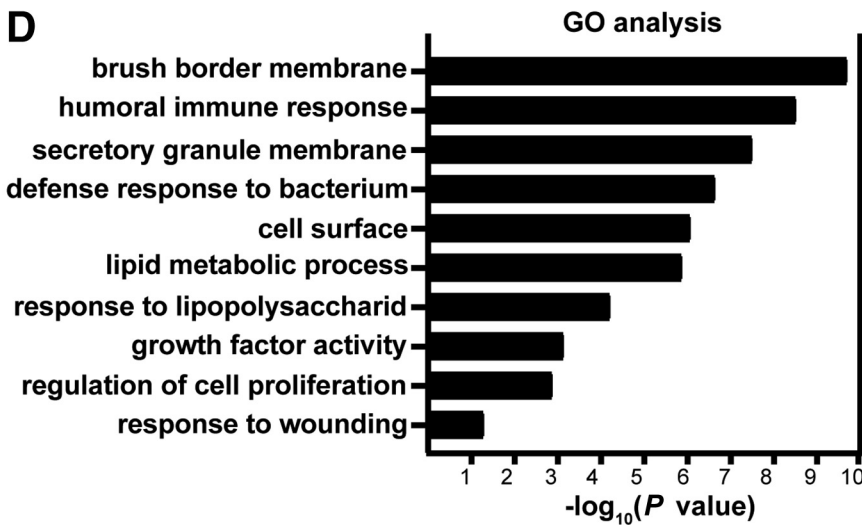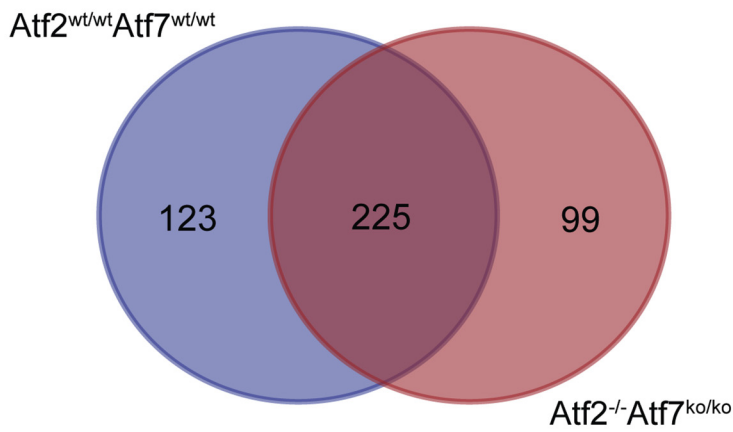
Organoid Culture and Viability

Isolation and culture of intestinal crypts were performed as described previously,[32] with adjustments made for colon tissue. In short, distal colon tissue, approximately 2 cm, was collected, from *Atf2$^{-/-}$/7$^{ko/ko}$* and *Atf2$^{wt/wt}$/7$^{wt/wt}$* mice, immediately after death. The tissue was cut open longitudinally, gently scraped with a coverslip, and washed with ice-cold PBS, and then incubated with 2 mmol/L EDTA in PBS on a rotating wheel. Residual debris was removed by gentle shaking, and the debris-containing supernatant was removed and replaced with cold PBS.

Figure 7. (*See previous page*). ATF2 and ATF7 are required to protect epithelial cells against TNF-induced death in organoid culture. Colonic epithelium was isolated from *Atf2$^{wt/wt}$Atf7$^{+/+}$* and *Atf2$^{-/-}$Atf7$^{ko/ko}$* mice and cultured as organoids (n = 3, independent organoid cultures). (*A*) qRT-PCR for the floxed region of *Atf2* and *Atf7* in colonic organoids. (*B*) Representative brightfield images of colonic organoids 72 hours after reseeding. (*C*) Quantification of organoid area and perimeter. (*D*) EdU incorporation assay using flow cytometry 72 hours after reseeding single cells (n = 3 for 2 independent experiments). (*E*) qRT-PCR for stem cell markers *Lgr5* and *Olfm4*. (*F*) PI viability assay on colon organoids challenged with TNF-α for 12 hours. *Scale bar*: 250 μm. Red fluorescence indicates cell death. (*G*) Percentage of nonviable organoids quantified per well (n = 2). Graph bars show means and SEM, **P < .01, ***P < .001, Student *t* test.

A

B

Upregulated genes upon TNF-alfa treatment

Atf2^(wt/wt)Atf7^(wt/wt)

123   225   99

Atf2^(-/-)Atf7^(ko/ko)

C

D

GO analysis

- brush border membrane
- humoral immune response
- secretory granule membrane
- defense response to bacterium
- cell surface
- lipid metabolic process
- response to lipopolysaccharid
- growth factor activity
- regulation of cell proliferation
- response to wounding

$-\log_{10}(P\ \text{value})$

This procedure was repeated until the supernatant was clear. After passing the supernatant through a cell strainer and centrifuge, the pellet was resuspended in 20 μL Matrigel (BD Biosciences) at a desired crypt density and plated in a 48-well plate. A total of 250 μL Epidermal Growth Factor, Noggin, Rspo1 (ENR)-culture medium was added, supplemented with 5 μmol/L glycogen synthase kinase-3 inhibitor CHIR-99021 (Axon, Groningen, Netherlands). Growth was assessed 3 days after repassaging organoids by measuring the perimeter and area surface using ImageJ software. To assess proliferation, we used the Click-iT EdU Flow Cytometry Assay kit (Thermo Fisher Scientific). First, EdU (20 μmol/L) was added on day 3 of colon organoid culture for 4 hours, then organoids were harvested and trypsinized. Subsequently, we followed the steps described in the manufacturer's protocol. We analyzed the cells with Flow Cytometry using 633-/635-nm excitation and a 660-/20-nm bandpass emission filter. For the recombinant mouse TNF-α exposure assay, colonic epithelial organoids plated in a 48-well plate were photographed and counted before and after treatment with recombinant mTNF-α at the budding stage after 2–3 days of culture using identical microscopic settings. A minimum of 100 crypts were counted over 2 culture wells (48-well plate), and defined as viable or dead by their morphologic appearance in the bright-field microscope and a nonviable/viable ratio was determined. mTNF-α was supplemented to culture medium in different concentrations for 12 hours to colon organoids. After 12 hours, the viability ratio again was determined and compared with pretreatment. Then, PI was added for 30 minutes to culture medium, and PI abundance subsequently was determined with a Leica DM6000 Digital Microscope equipped with LAS AF Software using appropriate fluorescence filters.

Electron Microscopy

Organoids of the small intestine and colon were harvested from $Atf2^{-/-}/7^{ko/ko}$ and $Atf2^{wt/wt}/7^{wt/wt}$ mice, immediately after 5 days of recombination and fixed in McDowell fixative containing 4% paraformaldehyde and 1% glutaraldehyde in 0.1 mol/L phosphate buffer. Organoids were postfixed with 1% osmium tetroxide (Electron Microscopy Sciences, Hatfield, PA) in cacodylate buffer. Subsequently, the samples were dehydrated in an alcohol series and embedded in epon (LX-112 resin; Ladd Research, Williston, VT). Then, 80-nm epon sections were cut and collected on formvar-coated grids, counterstained with uranyl acetate and lead citrate. Sections were examined using a Tecnai-12 G2 Spirit Biotwin electron microscope (Thermo Fisher, Eindhoven, The Netherlands), and images were taken using a Veleta camera with Radius software (EMSIS, Münster, Germany).

RNA Isolation, Complementary DNA Synthesis, and qRT-PCR

Intestinal tissue was lysed in 1 mL TRIzol (Thermo Fisher Scientific) and homogenized using small iron round balls. RNA extraction was performed according to the manufacturer's instructions. RNA from intestinal epithelial fraction or intestinal organoids was isolated using the RNAeasy mini kit (Qiagen, Hilden, Germany). For complementary DNA synthesis, 1 μg RNA was transcribed using Revertaid (Thermo Fisher Scientific, Waltham, MA). qRT-PCR was performed using SybrGreen (Roche) according to the manufacturer's protocol. Reference genes used for normalization according to the delta cycle threshold (ΔCt) method are as follows: in the homeostasis model for whole tissue we used *36B4* and *RPL32* as reference genes for colon and *36B4* and *Gapdh* as reference genes for small intestine. In the DSS model we used *HPRT* and *RPL4* as reference genes and for the organoid cultures we used *36B4* and *Ppib* as reference genes. Table 2 lists the primer sets used.

Cytokine Bead Array

Intestinal tissue was weighed and homogenized (100 mg tissue/mL) in cell lysis buffer (Cell Signaling Technology, Beverly, MA) with protease inhibitors (Roche) using Precellys tissue homogenizer tubes (Bertin Technologies, Montigny, France). For cytokine bead array, the BD Cytometric Bead Array Mouse Cytokine Kit (560485; BD Biosciences) was used according to the manufacturer's protocol. Concentrations in tissue lysates were corrected for total protein content as measured by BCA (Pierce, Thermo Fisher Scientific). The concentration of cytokines were determined by sandwich enzyme-linked immunoassay kit (DY460; R&D Systems, Minneapolis, MN).

Microarray

Colon organoids generated from $Atf2^{-/-}/7^{ko/ko}$ and $Atf2^{wt/wt}/7^{wt/wt}$ mice were plated in a 48-well plate. Per each organoid line, 8 wells were refreshed with ENR supplemented with mTNF-α at a concentration of 50 pg/mL and 8 wells were refreshed in normal ENR. After 12 hours, organoids were harvested for RNA isolation. RNA was isolated using the RNAeasy mini kit (Qiagen, Hilden, Germany) according to the manufacturer's instructions. RNA quality was measured on an Agilent (Palo Alto, CA) 2100 Bioanalyzer, and only samples with a RNA integrity number higher than 9 were included. For transcriptome profiling, 400 ng RNA was amplified and labeled using a 3′ IVT Nano Kit (Applied Biosystems, Foster City, CA) and an RNA Amplification Kit (Nugen, Redwood City, CA) according to the manufacturers' protocols. Microarray analysis of organoids was performed using an Affymetrix Clariom D 8-Array

Figure 8. (*See previous page*). **Gene expression analysis of $Atf2^{wt/wt}Atf7^{+/+}$ and $Atf2^{-/-}Atf7^{ko/ko}$ organoids.** (*A*) Principal component analyses (PCA) on global gene expression in $Atf2^{wt/wt}Atf7^{+/+}$ and $Atf2^{-/-}Atf7^{ko/ko}$ organoids at baseline and after 12 hours of TNF-α stimulation (n = 4 independent organoid cultures). (*B*) Venn diagram showing significantly up-regulated genes between $Atf2^{wt/wt}Atf7^{+/+}$ and $Atf2^{-/-}Atf7^{ko/ko}$ after TNF-α stimulation. (*C*) Curated heat maps of 99 up-regulated genes specific for $Atf2^{-/-}Atf7^{ko/ko}$ organoids. Highlighted genes were chosen based on biological interest. The *colored bar* represents the z-score–transformed expression level from low (red) to high (green). (*D*) Significantly altered GO pathways between $Atf2^{wt/wt}Atf7^{+/+}$ and $Atf2^{-/-}Atf7^{ko/ko}$ organoids on TNF-α stimulation.
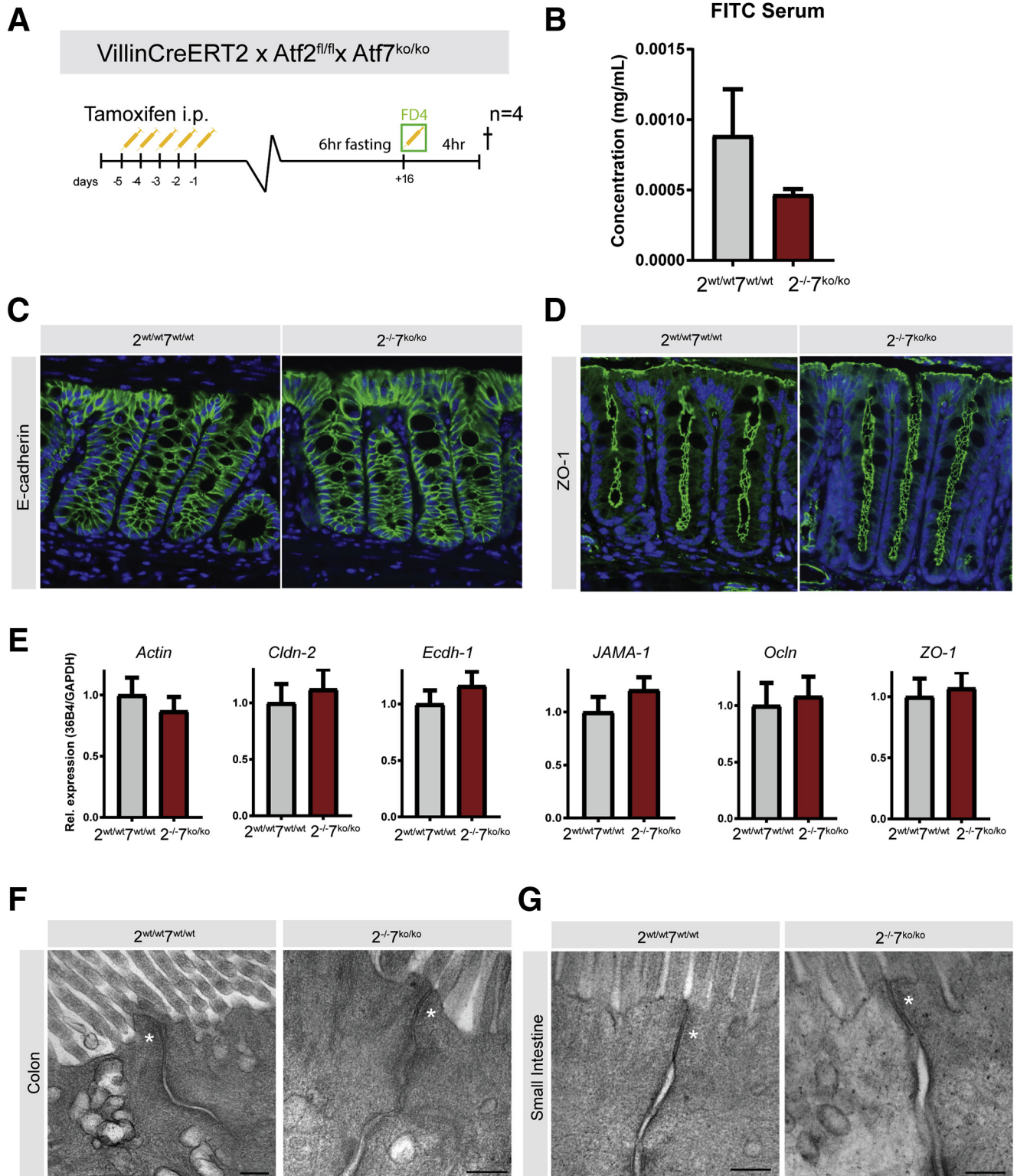
Figure 9. ATF2 and ATF7 are dispensable for intestinal barrier function under homeostatic conditions. (*A*) Four mice per group were induced by intraperitoneal injection with tamoxifen. Mice were fasted for 6 hours and then orally gavaged with FD4 (FITC dextran) dissolved in PBS. Four hours later, mice were killed (†) and cardiac puncture was performed to obtain blood. (*B*) Intestinal permeability assay measured by FITC fluorescence in serum. (*C*) E-cadherin immunofluorescence (green) in colon tissue with 4′,6-diamidino-2-phenylindole counterstain and (*D*) ZO-1 stain (green) in colon with 4′,6-diamidino-2-phenylindole counterstain (blue). (*E*) qRT-PCR for tight junction genes in mice under homeostatic conditions (n = 12 per group). (*F*) Electron microscopy of tight junctions in colon of control mice (*left panel*) and $Atf2^{-/-}/7^{ko/ko}$ (*right panel*), and (*G*) small intestine of control mice (*left panel*) or ATF mutant mice (*right panel*). *White asterisks* indicate tight junctions. *Scale bars*: 200 nm. GAPDH, glyceraldehyde-3-phosphate dehydrogenase; ZO-1, Zonula Occludens-1.

Table 1. Scoring System for DSS-Induced Colitis (Pathology Score)

Score	0	1	2	3	4
Area involved	0%	1%–10%	10%–25%	25%–50%	>50%
Follicles	Normal (0–1)	Minimal (2–3)	Mild (4–5)	Moderate (6–7)	Severe (>7)
Edema	Absent	Minimal	Mild	Moderate	Severe
Fibrosis	Absent	Minimal	Mild	Moderate	Severe
Erosion/ulceration	0%	1%–10%	10%–25%	25%–50%	>50%
Crypt loss	0%	1%–10%	10%–25%	25%–50%	>50%
Granulocytes	Normal	Minimal increase	Mild increase	Moderate increase	Severe increase
Mononuclear cells	Normal	Minimal increase	Mild increase	Moderate increase	Severe increase

HT Plate according to the standard protocols of the Dutch Genomics Service and Support Provider (MAD, Science Park, University of Amsterdam, Amsterdam, The Netherlands). The data were uploaded and normalized using R2: Genomics Analysis and Visualization Platform (available from: http://hgserver1.amc.nl). Differentially expressed genes were analyzed using Taq analysis and R2 software and selected based on fold change ($\geq$1.5), and a P value less than .05 in comparison with the control group.

Wound Healing (Scratch) Assay

Three-dimensional colon organoids were disrupted mechanically in cold advanced Dulbecco's modified Eagle medium to remove Matrigel. Subsequently, the pellet was resuspended in TrypLE (TrypLE Express, cat. 12605-010; Life Technologies, Carlsbad, CA) for 10 minutes at 37°C to obtain single cells. After counting, cells were plated at 200,000/well in ENR medium supplemented with CHIR-99021 (5 μmol/L; Axon, Groningen, Netherlands) and Rhok inhibitor (3.4 μg/mL, Y-27632 dihydrochloride

monohydrate; Sigma-Aldrich). After 24 hours of culture, cells were washed once with basal medium and refreshed with ENR medium supplemented with CHIR-99021 (5 μmol/L). Single cells then were seeded in a 12-well plate, precoated with Matrigel, and grown in a 2D monolayer. Once full confluence was reached, 2 scratches per well were made with a p10 pipet tip. Cell migration was filmed overnight with a Leica DMi8 inverted microscope, fitted with a humidified culture chamber maintained at 37°C, and the covered areas were quantified with ImageJ software.

Statistics

Statistical analysis was performed using Prism 7.0 (GraphPad Software, La Jolla, CA). All values are represented as the means ± SEM. Results were analyzed using the Student t test (Figures 1-7), the Mann–Whitney test (Figures 2 and 4), or 1-way analysis of variance followed by the Bonferroni post-test (Figure 6) as indicated throughout the figure legends. Differences were considered statistically significant at a P value less than .05.

Table 2. Primers Used for qRT-PCR Experiments

Gene	Forward primer	Reverse primer
Actin	GATGCTCCCCGGGCTGTATT	GGGGTACTTCAGGGTCAGGA
Alpl	TGGTCACAGCAGTTGGTAGC	TGACGTTCCGATCCTGAGTG
Ascl2	GAAGGTGCAAACGTCCACTT	TCCATCAAGCTTGCATTCAG
Atf2	GACTCCAACGCCAACAAGAT	AGGTAAAGGGCTGTCCTGGT
Atf2 (floxed exon)	CCAGCTCACACAACTCCTCA	GGACTGAACCCACACTTTCC
Atf7	AGACAGATTGTGGGACCGAG	CACAAACGGTCTGTCGTCTC
Atf7 (floxed exon)	CGGCGTACAGTGGATGAAGAT	CATTGCTAGGGGCTGATGCG
Cd44	TCTGCCATCTAGCACTAAGAGC	GTCTGGGTATTGAAAGGTGTAGC
Cdh1	GAGGTCTACACCTTCCCGGT	CCACTTTGAATCGGGAGTCT
ChgA	GTCTCCAGACACTCAGGGCT	ATGACAAAAGGGGACACCAA
Cldn15	GCTTCTTCATGTCAGCCCTG	TTCTTGGAGAGATCCATGTTGC
Cldn2	CCAGCCTCCAAGGGTTTCAT	TCTAGAAAACGGAGCCGTCC
Lgr5	TGTGTCAAAGCATTTCCAGC	CAGCGTCTTCACCTCCTACC
Lyz1	GGATGGCTACCGTGGTGTCAAGC	TCCCATAGTCGGTGCTTCGGTC
Muc2	GAAGCCAGATCCCGAAACCA	GAATCGGTAGACATCGCCGT
Olfm4	AACATCACCCCAGGCTACAG	TGTCCACAGACCCAGTGAAA
Sis	AGGTGTCCGCCTGAGCAAGGT	ATGGACGCCAGCAACAGCCA
Vil1	ATCTCCCTGAGGGTGTGGAC	AGAGAAGGCAGCTGGAGTCA
Zo1	AGGACACCAAAGCATGTGAG	GGCATTCCTGCTGGTTACA

References

1. Rescigno M. The intestinal epithelial barrier in the control of homeostasis and immunity. Trends Immunol 2011; 32:256–264.

2. de Sousa EMF, de Sauvage FJ. Cellular plasticity in intestinal homeostasis and disease. Cell Stem Cell 2019; 24:54–64.

3. Barker N. Adult intestinal stem cells: critical drivers of epithelial homeostasis and regeneration. Nat Rev Mol Cell Biol 2014;15:19–33.

4. Barker N, van Es JH, Kuipers J, Kujala P, van den Born M, Cozijnsen M, Haegebarth A, Korving J, Begthel H, Peters PJ, Clevers H. Identification of stem cells in small intestine and colon by marker gene Lgr5. Nature 2007;449:1003–1007.

5. Leedham SJ, Brittan M, McDonald SAC, Wright NA. Intestinal stem cells. J Cell Mol Med 2005;9:13.

6. Sato T, van Es JH, Snippert HJ, Stange DE, Vries RG, van den Born M, Barker N, Shroyer NF, van de Wetering M, Clevers H. Paneth cells constitute the niche for Lgr5 stem cells in intestinal crypts. Nature 2011; 469:415–418.

7. Sancho E, Batlle E, Clevers H. Signaling pathways in intestinal development and cancer. Annu Rev Cell Dev Biol 2004;20:695–723.

8. Nateri AS, Spencer-Dene B, Behrens A. Interaction of phosphorylated c-Jun with TCF4 regulates intestinal cancer development. Nature 2005;437:281–285.

9. Gupta J, del Barco Barrantes I, Igea A, Sakellariou S, Pateras IS, Gorgoulis VG, Nebreda AR. Dual function of p38alpha MAPK in colon cancer: suppression of colitis-associated tumor initiation but requirement for cancer cell survival. Cancer Cell 2014;25:484–500.

10. Shivers RP, Pagano DJ, Kooistra T, Richardson CE, Reddy KC, Whitney JK, Kamanzi O, Matsumoto K, Hisamoto N, Kim DH. Phosphorylation of the conserved transcription factor ATF-7 by PMK-1 p38 MAPK regulates innate immunity in Caenorhabditis elegans. PLoS Genet 2010;6:e1000892.

11. Vogt PK. Fortuitous convergences: the beginnings of JUN. Nat Rev Cancer 2002;2.

12. Huguier S, Baquet J, Perez S, vanDam H, Castelazzi M. Transcription factor ATF2 cooperates with v-Jun to promote growth factor-independent proliferation in vitro and tumor formation in vivo. Mol Cell Biol 1998;18:9.

13. Mandic AD, Bennek E, Verdier J, Zhang K, Roubrocks S, Davis RJ, Denecke B, Gassler N, Streetz K, Kel A, Hornef M, Cubero FJ, Trautwein C, Sellge G. c-Jun N-terminal kinase 2 promotes enterocyte survival and goblet cell differentiation in the inflamed intestine. Mucosal Immunol 2017;10:1211–1223.

14. Grumolato L, Liu G, Haremaki T, Mungamuri SK, Mong P, Akiri G, Lopez-Bergami P, Arita A, Anouar Y, Mlodzik M, Ronai ZA, Brody J, Weinstein DC, Aaronson SA. beta-Catenin-independent activation of TCF1/LEF1 in human hematopoietic tumor cells through interaction with ATF2 transcription factors. PLoS Genet 2013;9:e1003603.

15. Ouwens D, de Ruiter N, van der Zon G, Carter A, Schouten J, van der Burgt C, Kooistra K, Bos J, Maassen J, van Dam H. Growth factors can activate ATF2 via a two-step mechanism: phosphorylation of Thr71 through the Ras-MEK-ERK pathway and of Thr69 through RalGDS-Src-p38. EMBO J 2002;21:3782–3793.

16. Zhou W, Lin L, Majumdar A, Li X, Zhang X, Liu W, Etheridge L, Shi Y, Martin J, Van de Ven W, Kaartinen V, Wynshaw-Boris A, McMahon AP, Rosenfeld MG, Evans SM. Modulation of morphogenesis by noncanonical Wnt signaling requires ATF/CREB family-mediated transcriptional activation of TGFbeta2. Nat Genet 2007;39:1225–1234.

17. Schambony A, Wedlich D. Wnt-5A/Ror2 regulate expression of XPAPC through an alternative noncanonical signaling pathway. Dev Cell 2007;12:779–792.

18. Bhoumik A, Fichtman B, Derossi C, Breitwieser W, Kluger HM, Davis S, Subtil A, Meltzer P, Krajewski S, Jones N, Ronai Z. Suppressor role of activating transcription factor 2 (ATF2) in skin cancer. Proc Natl Acad Sci U S A 2008;105:9.

19. Hommes DW, Peppelenbosch MP, Van Deventer SJ. Mitogen activated protein (MAP) kinase signal transduction pathways and novel anti-inflammatory targets. Gut 2003;52:144–151.

20. Diegelmann J, Czamara D, Le Bras E, Zimmermann E, Olszak T, Bedynek A, Goke B, Franke A, Glas J, Brand S. Intestinal DMBT1 expression is modulated by Crohn's disease-associated IL23R variants and by a DMBT1 variant which influences binding of the transcription factors CREB1 and ATF-2. PLoS One 2013;8:e77773.

21. Maekawa T, Bernier F, Sato M, Nomura S, Singh M, Inoue Y, Tokunaga T, Imai H, Yokoyama M, Reimold A, Glimcher LH, Ishii S. Mouse ATF-2 null mutants display features of a severe type of meconium aspiration syndrome. J Biol Chem 1999;274:17813–17819.

22. Ackermann J, Ashton G, Lyons S, James D, Hornung JP, Jones N, Breitwieser W. Loss of ATF2 function leads to cranial motoneuron degeneration during embryonic mouse development. PLoS One 2011;6:e19090.

23. Reimold AM, Kim J, Finberg R, Glimcher LH. Decreased immediate inflammatory gene induction in activating transcription factor-2 mutant mice. Int Immunol 2001; 13:241–248.

24. Breitwieser W, Lyons S, Flenniken AM, Ashton G, Bruder G, Willington M, Lacaud G, Kouskoff V, Jones N. Feedback regulation of p38 activity via ATF2 is essential for survival of embryonic liver cells. Genes Dev 2007; 21:2069–2082.

25. Liu Y, Maekawa T, Yoshida K, Furuse T, Kaneda H, Wakana S, Ishii S. ATF7 ablation prevents diet-induced obesity and insulin resistance. Biochem Biophys Res Commun 2016;478:696–702.

26. Chassaing B, Aitken JD, Malleshappa M, Vijay-Kumar M. Dextran sulfate sodium (DSS)-induced colitis in mice. Curr Protoc Immunol 2014;104:15251–152514.

27. Booth C, Tudor G, Tudor J, Katz BP, MacVittie T. The acute gastrointestinal syndrome in high-dose irradiated mice. Health Phys 2012;103:383–399.

28. Beumer J, Clevers H. Regulation and plasticity of intestinal stem cells during homeostasis and regeneration. Development 2016;143:3639–3649.

29. Atreya R, Neurath MF. IBD pathogenesis in 2014: molecular pathways controlling barrier function in IBD. Nat Rev Gastroenterol Hepatol 2015;12:67–68.

30. Lopez-Posadas R, Neurath MF, Atreya I. Molecular pathways driving disease-specific alterations of intestinal epithelial cells. Cell Mol Life Sci 2017; 74:803–826.

31. Huang G, Shi LZ, Chi H. Regulation of JNK and p38 MAPK in the immune system: signal integration, propagation and termination. Cytokine 2009;48:161–169.

32. Sato T, Vries RG, Snippert HJ, van de Wetering M, Barker N, Stange DE, van Es JH, Abo A, Kujala P, Peters PJ, Clevers H. Single Lgr5 stem cells build crypt-villus structures in vitro without a mesenchymal niche. Nature 2009;459:262–265.

33. Van Lidth de Jeude JF, Vermeulen JL, Montenegro-Miranda PS, Van den Brink GR, Heijmans J. A protocol for lentiviral transduction and downstream analysis of intestinal organoids. J Visualized Exp 2015;98:1–11.

34. Van der Sluis M, De Koning BA, De Bruijn AC, Velcich A, Meijerink JP, Van Goudoever JB, Buller HA, Dekker J, Van Seuningen I, Renes IB, Einerhand AW. Muc2-deficient mice spontaneously develop colitis, indicating that MUC2 is critical for colonic protection. Gastroenterology 2006;131:117–129.

35. el Marjou F, Janssen KP, Chang BH, Li M, Hindie V, Chan L, Louvard D, Chambon P, Metzger D, Robine S. Tissue-specific and inducible Cre-mediated recombination in the gut epithelium. Genesis 2004; 39:186–193.

36. Cooper HS, Murthy SN, Shah RS, Sedergran DJ. Clinicopathologic study of dextran sulfate sodium experimental murine colitis. Lab Invest 1993;69:238–249.

Correspondence
Address correspondence to: Bartolomeus Meijer, MD, Department of Gastroenterology and Hepatology, AG&M, Tytgat Institute for Liver and Intestinal Research, University of Amsterdam, Meibergdreef 69-71, 1105 BK, Amsterdam, The Netherlands. e-mail: b.j.meijer@amsterdamumc.nl; fax: (020) 5669190.